

This work has been published in Nature Cell Biology, Aug 15, 2010 [Epub ahead of print].  
DOI: 10.1038/ncb2092

## Live imaging RNAi screen identifies PP2A-B55 $\alpha$ and Importin $\beta$ 1 as key mitotic exit regulators in human cells

Michael H. A. Schmitz<sup>1,2,3</sup>, Michael Held<sup>1,2</sup>, Veerle Janssens<sup>4</sup>, James R. A. Hutchins<sup>5</sup>, Otto Hudecz<sup>6</sup>, Elitsa Ivanova<sup>4</sup>, Jozef Goris<sup>4</sup>, Laura Trinkle-Mulcahy<sup>7</sup>, Angus I. Lamond<sup>8</sup>, Ina Poser<sup>9</sup>, Anthony A. Hyman<sup>9</sup>, Karl Mechtler<sup>5,6</sup>, Jan-Michael Peters<sup>5</sup>, and Daniel W. Gerlich<sup>1,2,10</sup>

<sup>1</sup>Institute of Biochemistry, Swiss Federal Institute of Technology Zurich (ETHZ), Schafmattstr. 18, CH-8093 Zurich, Switzerland

<sup>2</sup>Marine Biological Laboratory, Woods Hole, MA 02543, USA

<sup>3</sup>Current address: Systems and Cell Biology of Neurodegeneration, Division of Psychiatry Research, University of Zurich, August Forel-Strasse 1, CH-8008 Zurich, Switzerland

<sup>4</sup>Laboratory of Protein Phosphorylation and Proteomics, Dept. of Molecular Cell Biology, Faculty of Medicine, KU Leuven, Gasthuisberg O&N1, Herestraat 49 Box 901, B-3000 Leuven, Belgium.

<sup>5</sup>Institute of Molecular Pathology, Dr. Bohr-Gasse 7, 1030 Vienna, Austria

<sup>6</sup>Institute of Molecular Biotechnology of the Austrian Academy of Sciences, Dr. Bohr-Gasse 3, 1030 Vienna, Austria

<sup>7</sup>Department of Cellular & Molecular Medicine and the Ottawa Institute of Systems Biology, University of Ottawa, 451 Smyth Road, Ottawa, ON K1H 8M5, Canada

<sup>8</sup>Wellcome Trust Centre for Gene Regulation & Expression, MSI/WTB/JBC Complex, University of Dundee, Dundee DD1 5EH, UK.

<sup>9</sup>Max-Planck-Institute for Molecular Cell Biology and Genetics, Pfotenhauerstrasse 108, D-01307 Dresden, Germany

<sup>10</sup>Correspondence should be addressed to: D.W.G. (daniel.gerlich@bc.biol.ethz.ch)

**When vertebrate cells exit mitosis, they reorganize various cellular structures to build functional interphase cells<sup>1</sup>. This depends on Cdk1 inactivation and subsequent dephosphorylation of its substrates<sup>2-4</sup>. Members of PP1 and PP2A phosphatase families can dephosphorylate Cdk1 substrates in biochemical extracts during mitotic exit<sup>5, 6</sup>, but how this relates to postmitotic reassembly of interphase structures in intact cells is not known. Here, we used a live imaging assay to screen by RNAi a genome-wide library of protein phosphatases for mitotic exit functions in human cells. We identified a trimeric PP2A-B55α complex as a key factor for postmitotic reassembly of the nuclear envelope, the Golgi apparatus, and decondensed chromatin, as well as for mitotic spindle breakdown. Using a chemically-induced mitotic exit assay, we found that PP2A-B55α functions downstream of Cdk1 inactivation. PP2A-B55α isolated from mitotic cells had reduced phosphatase activity towards the Cdk1 substrate histone H1 and it was hyper-phosphorylated on all subunits. Mitotic PP2A complexes co-purified with the nuclear transport factor Importin β1, and RNAi depletion of Importin β1 delayed mitotic exit synergistically with PP2A-B55α. This demonstrates that PP2A-B55α and Importin β1 cooperate in the regulation of postmitotic assembly mechanisms in human cells.**

In budding yeast, Cdk1 substrate dephosphorylation and mitotic exit depend on the Cdc14 phosphatase<sup>7</sup>, but this function does not seem to be conserved in Cdc14 homologues of other species<sup>2, 3, 8-11</sup>. Studies in cycling *Xenopus* embryonic extracts suggest that phosphatases of both PP1<sup>5</sup> and PP2A<sup>6</sup> families can contribute to Cdk1 substrate dephosphorylation during vertebrate mitotic exit, whereas Ca<sup>2+</sup>-triggered mitotic exit from cytostatic factor-arrested egg extracts depends on calcineurin<sup>12, 13</sup>. Early genetic studies in *Drosophila melanogaster*<sup>14, 15</sup> and *Aspergillus nidulans*<sup>16</sup> reported late mitotic defects for PP1 and PP2A mutants. However, the assays used in these studies were not specific for mitotic exit, because they scored prometaphase arrest or anaphase chromosome bridges, which can result from earlier mitotic defects.

Intracellular targeting of serine/threonine phosphatase complexes to specific substrates is mediated by association of a small group of common catalytic subunits with a diverse spectrum of regulatory/targeting subunits<sup>3, 4, 17</sup>. It is possible that mitotic exit in intact cells requires phosphatases that have not been detected with previous assays using *in vitro* extracts. In practice, the short duration of mitotic exit makes it difficult to assay this process, which explains why previous RNAi screening on cell division regulators<sup>18</sup> did not annotate mitotic exit phenotypes.

To assay mitotic exit in live human cells, we measured the timing from anaphase onset until nuclear reformation. We generated a HeLa cell line stably expressing a chromatin marker (histone 2B fused to a red fluorescent protein; H2B-mCherry<sup>19</sup>) to visualize the metaphase - anaphase transition (Fig. 1a-c). To probe for postmitotic nuclear reassembly, we stably co-expressed a nuclear import substrate (importin β-binding domain of importin α fused to monomeric EGFP; IBB-mEGFP<sup>20</sup>), which is cytoplasmic in mitosis, and co-localizes with chromatin regions after reassembly of a functional nuclear envelope (Fig. 1a, b).

To annotate mitotic exit timing automatically in time-lapse movies, we used in house-developed computational methods (*CellCognition*<sup>21</sup>). Individual cells were detected and tracked over time, and the mitotic stage of each cell was assigned based on classification of chromatin morphology (Fig. 1c). Nuclear breakdown and reassembly was determined based on the ratio of mean IBB-mEGFP fluorescence on chromatin regions versus surrounding cytoplasmic regions (Fig. 1d). Automated annotation of mitotic exit timing ( $4.70 \pm 0.89$  min; mean $\pm$ s.d.) closely matched manual annotation ( $4.88 \pm 0.84$  min; mean $\pm$ s.d.; n = 270 cells, see Supplementary Information, Fig. S1).

We next imaged cells over ~24 h with time-intervals of ~3.8 min after transfection of 675 different siRNAs targeting a genome-wide set of 225 annotated human protein phosphatases, including catalytic and associated regulatory and scaffolding subunits (3 different siRNAs per gene, two technical replicas; full list of siRNAs see Supplementary Information, Table 1). On average, this yielded ~87 automatically annotated mitotic events per movie (total: 113,236 mitotic events). We determined the mean mitotic exit timing for all data sets that contained more than 10 mitotic events (n = 1,278 out of the 1,350 movies). Five siRNAs reproducibly scored as hits above a significance cut-off at three standard deviations above the mean of all data points (z-score = 3; Fig. 2a). These five siRNAs

targeted three distinct genes, encoding each of the three subunits of a heterotrimeric PP2A complex, PPP2CA (catalytic subunit alpha, subsequently labelled as “CA”), PPP2R1A (scaffold subunit alpha, subsequently labelled as “R1A”), and PPP2R2A (regulatory B-type subunit, also termed PR55 $\alpha$  or B55 $\alpha$ , subsequently labelled as “B55 $\alpha$ ”). The remaining four siRNAs targeting the same PP2A genes also prolonged mitotic exit, albeit below the cut-off level (Fig. 2a).

To validate the hits, we tested an extended set of 6 siRNAs per gene, which all significantly ( $p < 0.001$ ; t-test) prolonged mitotic exit (Supplementary Information, Fig. S2a-c). The mRNA depletion levels correlated with phenotypic penetrance (Supplementary Information, Fig. S2a-f), indicating specificity of the phenotype. The RNAi depletion was also efficient at the protein level (Supplementary Information, Fig. S2g). We next depleted endogenous B55 $\alpha$  in a HeLa cell line stably expressing EGFP-tagged mouse B55 $\alpha$ . Transfection of a siRNA targeting a non-conserved sequence on the human B55 $\alpha$  mRNA efficiently depleted endogenous B55 $\alpha$ , but not the exogenous mouse B55 $\alpha$  (Fig. 2b), and these cells showed normal mitotic exit timing (Fig. 2c). In contrast, transfection of a siRNA targeting both human and mouse B55 $\alpha$  mRNA, or R1A, in these cells efficiently delayed mitotic exit (Fig. 2c). This validates that the observed phenotype was caused by on-target depletion of B55 $\alpha$  mRNA.

The family of PP2A protein phosphatases is involved in many cellular processes, including earlier mitotic stages<sup>3</sup>. It is generally believed that the regulatory B-type subunit confers substrate specificity and thereby regulates diverse functions of PP2A<sup>3,17</sup>. Depletion of CA or R1A significantly ( $p < 0.001$ ; t-test) prolonged mitotic progression from nuclear envelope breakdown until anaphase (Fig. 2d; same cells shown in Fig. 2e), as expected from the known functions of PP2A complexes involving other B-type subunits in spindle assembly and chromosome cohesion<sup>3</sup>. In contrast, early mitotic progression was unaffected in B55 $\alpha$ -depleted cells. These data indicate that PP2A function is required at all stages of mitosis, whereas the B55 $\alpha$  subunit is rate-limiting only for post-anaphase progression.

Cells depleted for PP2A-B55 $\alpha$  subunits were delayed but not arrested during mitotic exit (Fig. 2e). This may be explained by incomplete RNAi depletion or involvement of other unknown factors with redundant function. To investigate if additional phosphatases become limiting in the absence of B55 $\alpha$ , we screened the phosphatase-targeting siRNA library in a background of synthetic B55 $\alpha$  RNAi depletion. Increased mitotic exit delay occurred upon co-depletion of R1A or CA subunits with B55 $\alpha$  (2/3 oligos scoring above a z-score threshold of 3; Fig. 2f). However, none of the other 222 phosphatases showed consistent additive phenotype increase (5 other siRNA oligos delayed slightly above the z-score threshold, but could not be confirmed by different siRNAs targeting the same genes). Co-transfection of siRNAs targeting all three PP2A-B55 $\alpha$  subunits (labelled as siPP2A-B55 $\alpha$  throughout the manuscript) caused the most pronounced prolongation of mitotic exit ( $14.76 \pm 6.50$  min versus  $4.86 \pm 1.07$  min in control; mean $\pm$ s.d.;  $n \geq 205$ ; Fig. 2g; Supplementary Information, Fig. S2g). The additive effect of combinatorial PP2A-B55 $\alpha$  subunit depletions suggests that residual levels of this phosphatase may account for a slow and gradual mitotic exit. That no other RNAi conditions further delayed mitotic exit in combination with B55 $\alpha$  depletion underlines the particular importance of PP2A-B55 $\alpha$  for mitotic exit.

To address if PP2A-B55 $\alpha$  controls postmitotic reassembly of cellular structures other than the nucleus, we generated a HeLa cell line stably expressing a fluorescent Golgi marker (galactosyl transferase, GalT-mEGFP<sup>22</sup>) and H2B-mCherry (Fig. 3a). Confocal time-lapse microscopy showed that depletion of the PP2A-B55 $\alpha$  complex significantly ( $p < 0.001$ ; t-test) delayed postmitotic clustering of Golgi fragments (Fig. 3a, b, e;  $25.5 \pm 5.86$  min versus  $11.17 \pm 2.73$  min in control; mean $\pm$ s.d.;  $n \geq 30$ ; for single depletion of B55 $\alpha$  see Supplementary Information, Fig. S3b, c). In another mitotic exit assay, we imaged a HeLa cell line stably expressing H2B-mCherry and mEGFP- $\alpha$ -tubulin<sup>19</sup> (Fig. 3c). PP2A-B55 $\alpha$ -depleted cells showed significantly delayed disassembly of spindle pole-associated microtubules (Fig. 3c, d, f). Postmitotic chromosome decondensation was also significantly ( $p < 0.001$ ; t-test) delayed in PP2A-B55 $\alpha$ -depleted cells ( $18.29 \pm 2.29$  min versus  $8.94 \pm 5.89$  min in control; mean $\pm$ s.d.;  $n \geq 97$ ; see also Supplementary Information Fig. S3d). These data show that PP2A-B55 $\alpha$  contributes to postmitotic reassembly of various interphase cell structures.

We next investigated how PP2A-B55 $\alpha$  depletion affected progression through interphase, using a monoclonal cell line expressing H2B-mCherry and a DNA replication marker (EGFP-PCNA<sup>23</sup>;

Supplementary Information, Fig. S4a-d). PP2A-B55 $\alpha$ -depleted cells were prolonged in G1 ( $8.00 \pm 2.09$  h versus  $5.77 \pm 1.11$  h in control; mean $\pm$ s.d.; n  $\geq 39$ ; Supplementary Information, Fig. S4b), as expected after perturbed mitotic exit. On the other hand, PP2A-B55 $\alpha$ -depleted cells had a significantly ( $p < 0.001$ ; t-test) shorter G2 phase ( $2.91 \pm 0.39$  h versus  $3.95 \pm 0.78$  h in control; mean $\pm$ s.d.; n  $\geq 38$ ; Supplementary Information, Fig. S4d). This is consistent with previous observations in *Xenopus* embryonic extracts<sup>6, 24</sup>.

The mitotic exit phenotypes observed after PP2A-B55 $\alpha$  depletion could be due either to a failure in Cdk1 inactivation, or to misregulated Cdk1 substrate dephosphorylation, or both. To discriminate between these possibilities, we established a mitotic exit assay using chemical inactivation of Cdk1. Cells were first arrested in metaphase by the proteasome inhibitor MG132 and then forced to exit from mitosis by adding the Cdk inhibitor flavopiridol to 20  $\mu$ M final concentration, still in the presence of MG132<sup>25</sup> (Fig. 4a). This efficiently promoted most hallmarks of physiological mitotic exit, including nuclear reassembly (>95% of all metaphase cells; n = 99), Golgi clustering (>90%; n = 103), chromosome decondensation, and re-attachment of the cells to the substratum (Fig. 4b, d). Only chromosome segregation did not occur, presumably due to the suppression of securin degradation by MG132. Higher concentrations of flavopiridol did not further accelerate nuclear reassembly ( $9.4 \pm 1.1$  min at 160  $\mu$ M compared to  $9.3 \pm 1.3$  min at 20  $\mu$ M; mean $\pm$ s.d.; n  $\geq 30$ ), indicating that Cdk1 inhibition was complete. PP2A-B55 $\alpha$  depletion significantly ( $p < 0.001$ ; t-test) delayed nuclear reassembly in this assay ( $20.67 \pm 3.30$  min versus  $9.86 \pm 0.95$  min in control; mean $\pm$ s.d.; n  $\geq 29$ ; Fig. 4b, c, f; for single depletion of B55 $\alpha$ , see Supplementary Information, Fig. S5a-c). Golgi reformation was also delayed ( $36.01 \pm 9.38$  min versus  $16.91 \pm 2.27$  min in control; n  $\geq 35$ ; Fig. 4d, e, g). We conclude that a main function of PP2A-B55 $\alpha$  in promoting mitotic exit must be downstream of Cdk1 inactivation.

To test if PP2A-B55 $\alpha$  depletion affected Cdk1 substrate dephosphorylation, we prepared extracts from HeLa cells synchronized to different time points after chemical induction of mitotic exit. Cdk1 substrate phosphorylation, detected on quantitative Western Blots by an anti-phospho-serine antibody that specifically recognizes the Cdk target sequence (K/R) pS PX (K/R) (pS = phospho-serine), dropped to ~23% within 18 min in negative controls, whereas it remained at ~66% in PP2A-B55 $\alpha$ -depleted cells (Fig. 4h; for single depletion of B55 $\alpha$  see Supplementary Information, Fig. S5e). This substantiates the conclusion that PP2A-B55 $\alpha$  functions downstream of Cdk inactivation during mitotic exit and shows that PP2A-B55 $\alpha$  is required for timely Cdk1 substrate dephosphorylation.

Previous studies in *Xenopus* embryonic extracts<sup>5, 13</sup> and HeLa cells<sup>26</sup> indicated reduced phosphatase activity towards Cdk1 targets during early mitosis. Human PP2A-B55 $\alpha$  isolated from mitotic cells had significantly reduced activity towards Cdk1-phosphorylated histone H1 (Fig. 5a;  $71 \pm 15\%$  versus  $100 \pm 11\%$  in interphase, mean $\pm$ s.d.; n = 15;  $p < 0.001$ ; t-test). However, we did not detect any cell cycle-dependent differences in the phosphatase activity towards another well-characterized model substrate, phosphorylase  $\alpha$  (Fig. 5b). This suggests cell cycle-regulated changes of PP2A-B55 $\alpha$  substrate specificity.

All three PP2A-B55 $\alpha$  subunits were expressed at similar levels in interphase and mitosis (Supplementary Information, Fig. S6a), suggesting that mitotic PP2A-B55 $\alpha$  is unlikely to be regulated at the protein level. We addressed potential changes in PP2A complex composition at different cell cycle stages by purification of Localization and Affinity Purification (LAP)-tagged R1A or B55 $\alpha$  stably expressed from endogenous promoters<sup>27</sup>. R1A co-purified with several mitosis-specific binding partners (Fig. 5c), two of which were identified by mass spectrometry as the nuclear transport factors Importin  $\alpha 1$  and Importin  $\beta 1$ . Besides the function in nuclear transport during interphase, Importin  $\beta 1$  is part of a mitotic regulatory system involving the small GTPase Ran, which is known to control mitotic spindle and nuclear envelope assembly<sup>28</sup>. After validation of the mitosis-specific interaction between Importin  $\beta 1$  and R1A by Western Blotting (Fig. 5d), we investigated if Importin  $\beta 1$  contributes to mitotic exit progression. Because the specificity of the nuclear reassembly assay may be compromised after depletion of a nuclear import factor, we assayed mitotic exit by Golgi reformation. Importin  $\beta 1$  depletion (Supplementary Information, Fig. S2h, i) significantly delayed postmitotic Golgi reassembly (Fig. 5e;  $14.7 \pm 5.0$  min versus  $10.1 \pm 1.4$  min in control; mean $\pm$ s.d.; n  $\geq 30$ ;  $p \leq 0.001$ ), which was further increased after co-transfection of siRNAs targeting R1A or B55 $\alpha$  ( $25.9 \pm 6.3$  min, and  $22.5 \pm 8.1$  min, respectively). Importin  $\beta 1$  depletion also prolonged earlier mitotic

stages (Supplementary Information, Fig. S7), as expected from its known function in spindle assembly. These data demonstrate that PP2A-B55 $\alpha$  and Importin  $\beta$ 1 jointly promote mitotic exit.

By mass spectrometry, we detected five phosphorylation sites on the PP2A complex purified from mitotic cells (Fig. 5f). We estimated the relative quantities of phosphopeptides by a semi-quantitative approach, using the extracted ion chromatogram for peak area quantitation of the peptide elution profiles (Supplementary Information, Fig. S8). S167 phosphorylation on B55 $\alpha$  was estimated highly abundant at 55% (mean; n = 2 independent experiments), whereas the other sites were phosphorylated on <1% of the eluted peptides (quantifications provided in Fig. 5f; the phosphorylation levels of S8 on R1A could not be determined because no unmodified peptides containing this site were detected). PP2A is known to auto-dephosphorylate<sup>29</sup>, therefore the absolute phosphorylation levels in cells may be higher. All of the four quantified phosphorylations were enriched more than 5-fold on PP2A purified from mitotic cells (Fig. 5f; Supplementary Information, Fig. S8). To test if the most abundant mitotic phosphorylation, S167 on B55 $\alpha$ , contributes to the regulation of PP2A complex assembly, we expressed GST-tagged phospho-mimicking S167E mutant of B55 $\alpha$  for isolation of PP2A complexes from interphase and mitotic HeLa cells. Indeed, the S167E mutant bound less efficiently to the CA and R1A subunits, as compared to wildtype B55 $\alpha$ , or a non-phosphorylatable S167A mutant (Fig. 5g; Supplementary Information, Fig. S9h).

To the best of our knowledge, this study provides the first comprehensive screen for mitotic exit phosphatases in human cells. B55 $\alpha$  has been previously shown to increase PP2A activity towards Cdk1 phosphorylation sites<sup>30</sup>, consistent with the possibility that PP2A-B55 $\alpha$  promotes mitotic exit by direct dephosphorylation of Cdk1 substrates. The *in vitro* phosphatase activity of mitotic PP2A-B55 $\alpha$  towards Cdk1-phyosphorylated H1 was downregulated. However, it is not known which of the many putative PP2A substrates may be affected by this regulation, and we therefore cannot precisely estimate the extent by which PP2A regulation shapes the kinetics of Cdk1 substrate dephosphorylation.

Our data raise interesting possibilities for PP2A regulatory mechanisms (Fig. 5h). Phospho-mimicking S167E mutation on B55 $\alpha$  impaired the binding of R1A and CA subunits, consistent with the possibility that phosphorylation contributes to a cell cycle-dependent regulation of PP2A-B55 $\alpha$  complex assembly. This may further involve mitotic CA-T304 hyper-phosphorylation, as a previous study showed that a phospho-mimicking CA-T304D mutation also suppresses assembly of B55 $\alpha$  into PP2A complexes<sup>31</sup>. Importin  $\beta$ 1 may regulate PP2A by direct binding, by a nuclear-cytoplasmic targeting mechanism, or as a molecular chaperone<sup>28</sup>. In this context, it is interesting to note that Importin  $\beta$ 1 is structurally related to the R1A subunit and members of the B' family of regulatory PP2A subunits<sup>32</sup>. Even though it is possible that Importin  $\beta$ 1 functions in a mitotic exit pathway independently of PP2A, the here observed physical and functional interaction suggests a link between the Importin/Ran and Cdk1-phosphorylation regulatory systems.

In contrast to the *Xenopus* embryonic extract system<sup>6</sup>, depletion of B55 $\delta$  in HeLa cells (down to 20% mRNA level; Supplementary Information, Fig. S2j) did not delay mitotic exit. This may reflect different relative expression levels of the B55-subfamily isoforms in the two systems or technical limitations of the depletion methods. A previous study proposed that PP1 dominates as a Cdk1-counteracting phosphatase in cycling *Xenopus* embryonic extracts<sup>5</sup>. That we did not detect mitotic exit delays after RNAi depletion of any of the PP1 catalytic or regulatory subunits may be due to the cellular context of our phenotypic assays instead of homogenized extracts, or to differences between embryonic and somatic mitosis. However, potential functional redundancy between different PP1 catalytic isoforms that were targeted only individually in our screen may have masked phenotypes and we therefore cannot rule out that PP1 also contributes to mitotic exit in human somatic cells.

In conclusion, our study reveals PP2A-B55 $\alpha$  and Importin  $\beta$ 1 as key regulators of cellular reassembly mechanisms during mitotic exit. Mitotic exit has been recently recognized as a target for improved, next-generation cancer therapeutics<sup>33</sup>. B55 $\alpha$  and Importin  $\beta$ 1 are therefore good target protein candidates for the development of mitotic exit-specific inhibitors.

## Acknowledgments

The authors thank F. Uhlmann and B. Novak for critical comments on the manuscript. We thank S. Maar, the ETHZ Light Microscopy Centre (LMC) and the ETHZ RNAi Screening Centre (RISC), M. Augsburg (MPI-CBG), M. Leuschner (MPI-CBG), and A. Ssykor (MPI-CBG) for excellent technical assistance. We thank U. Kutay (ETHZ) for anti-Importin  $\beta$ 1 and anti-nucleolin antibodies, J. Rohrer (University Zurich) for providing Galt-EGFP plasmid, J. Ellenberg (EMBL Heidelberg) for IBB-EGFP, M.C. Cardoso (Technical University Darmstadt) for EGFP-PCNA plasmid, and Sanofi Aventis and the National Cancer Institute for providing Flavopiridol. This work was supported by SNF research grant 3100A0-114120, SNF ProDoc grant PDFMP3\_124904, a European Young Investigator (EURYI) award of the European Science Foundation to DWG, and a MBL Summer Research Fellowship by the Evelyn and Melvin Spiegel Fund to DWG, a Roche Ph.D. fellowship to MHAS, and a Mueller fellowship of the Molecular Life Sciences Ph.D. program Zurich to MH. MH and MHAS are fellows of the Zurich Ph.D. Program in Molecular Life Sciences. VJ and JG were supported by grants of the ‘Geconcerdeerde OnderzoeksActies’ of the Flemish government, the ‘Interuniversitary Attraction Poles’ of the Belgian Science Policy P6/28 and the ‘Fonds voor Wetenschappelijk Onderzoek-Vlaanderen’. AIL is a Wellcome Trust Principal Research Fellow. AAH acknowledges funding by the Max Planck Society, the EU-FP6 integrated project MitoCheck, and the BMBF grant DiGtoP [01GS0859]. Work in the groups of KM and JMP was supported by the EU-FP6 integrated project MitoCheck, Boehringer Ingelheim and by the GEN-AU programme of the Austrian Federal Ministry of Science and Research (Austrian Proteomics Platform III), by MeioSys within the Seventh Framework Programme of the European Commission, and by Chromosome Dynamics, which is funded by the Austrian Science Foundation (FWF).

## Author contributions

MHAS performed all experiments except of the mass spectrometry and *in vitro* phosphatase assays, and wrote part of the paper. MH implemented software for automated imaging and data analysis. VJ, EI, and JG performed *in vitro* phosphatase assays and B55 $\alpha$  phospho-mutant analysis. JH and JMP designed and performed PP2A purification. KM and OH performed mass spectrometry. LTM and AIL compiled the phosphatase screening library. IP and AAH generated the cell lines stably expressing LAP-tagged PP2A subunits. DWG conceived the project, designed the screening strategy, and wrote the paper.

## Figure legends

**Figure 1. Live imaging assay for mitotic exit timing.** **(a)** Automated time-lapse imaging of HeLa cell line stably expressing a chromatin marker (H2B-mCherry; red) and a nuclear import substrate IBB-EGFP (green). The selected images show about 13% of the movie field-of-view. See Supplementary Information, Movie S1. **(b)** Single cell progressing through mitosis. **(c)** Automated detection of chromatin regions, tracking of cells over time, and annotation of mitotic stages by supervised machine learning and classification of chromatin morphologies. See Supplementary Information, Movie S2. **(d)** Automated detection of nuclear breakdown and reassembly. Chromatin regions (red) were defined by automated segmentation of the chromatin fluorescence (see Fig. 1c). Cytoplasmic regions (green indicates outer boundary, red is inner boundary) were derived by dilation of the chromatin regions. The ratio of mean IBB-EGFP fluorescence in chromatin / cytoplasm regions served to automatically determine nuclear envelope breakdown (orange bar) and reformation after anaphase (IBB onset, blue bar). Anaphase onset was defined by the classification of chromatin morphology (violet bar, see (c)). Scale bars: 10  $\mu$ m.

**Figure 2. RNAi screen for mitotic exit regulators.** (a) RNAi screen of a genome-wide library of annotated protein phosphatases using the mitotic exit assay shown in Fig. 1. Individual data points correspond to the z-score based on the mean mitotic exit timing in individual movies, determined in two technical replicas. Negative controls are black. SiRNA oligos causing phenotypes reproducibly scoring above a z-score threshold of  $> 3$  (dashed lines) were considered as hits (highlighted by colours as indicated in legend; siRNAs targeting the same genes as the hits but with z-scores below threshold are also highlighted). (b) RNAi depletion of B55 $\alpha$  in a HeLa cell line stably expressing localization-and-affinity (LAP)-tagged mouse-B55 $\alpha$  from a bacterial artificial chromosome (BAC; for localization see Supplementary Information, Fig. S6b). Cells were transfected with siRNA targeting either human B55 $\alpha$  alone (h), or both human- and mouse-B55 $\alpha$  (m/h). Quantitative Western Blot probing with anti-B55 $\alpha$  antibody that recognizes both mouse and human B55 $\alpha$ . (c) Rescue of mitotic exit delay phenotype by exogenous B55 $\alpha$ . Mouse-B55 $\alpha$ -LAP cells were RNAi-depleted for human (h) or both human/mouse (m/h) B55 $\alpha$ , as validated in (b). (d) Cumulative histograms for early mitotic progression. Nuclear envelope breakdown (NEBD) until anaphase onset was measured in control and RNAi-depleted cells ( $n \geq 64$  in all conditions). (e) Cumulative histograms of mitotic exit. Anaphase onset until nuclear import of IBB-EGFP was measured for the same cells shown in (d). (f) Synthetic depletion RNAi screen for mitotic exit phosphatases. Assay, sample preparation, and siRNA library was identical to the screen shown in (a), except that siRNA targeting B55 $\alpha$  was co-transfected in each experimental condition. Negative controls (black) were only transfected by non-targeting siRNA. The plot shows the ranked z-scores of a single replica, calculated as in (a). Dashed line indicates z-score threshold. (g) Time-lapse images of a cell depleted of all three PP2A-B55 $\alpha$  subunits progressing through mitotic exit, full movie shown in Supplementary Information, Movie S4. For negative control, see Supplementary Information, Movie S3. Scale bars: 10  $\mu$ m.

**Figure 3. PP2A-B55 $\alpha$  controls postmitotic Golgi assembly, spindle breakdown and chromatin decondensation.** (a) Confocal time-lapse movie of a control cell expressing H2B-mCherry and the Golgi marker GalT-EGFP, see Supplementary Information, Movie S5. Golgi reassembly was scored based on clustering into two distinct patches per cell ( $t = 9$  min). (b) Golgi reassembly in a PP2A-B55 $\alpha$ -depleted cell, see Supplementary Information, Movie S6. (c) Confocal time-lapse images of mitotic spindle disassembly and chromosome decondensation in a control cell, see also Supplementary Information, Movie S7. Spindle disassembly was scored based on the first apparent detachment of spindle pole-associated microtubules from chromatin masses ( $t = 9$  min). (d) Mitotic spindle disassembly in a PP2A-B55 $\alpha$ -depleted cell, see Supplementary Information, Movie S8. (e, f) Cumulative histograms of postmitotic Golgi clustering (e), or spindle disassembly (f) relative to anaphase onset ( $t = 0$  min). Scale bars: 10  $\mu$ m.

**Figure 4. PP2A-B55 $\alpha$  functions downstream of Cdk1 inactivation.** (a) Experimental protocol for mitotic exit induced by chemical inactivation of Cdks in absence of proteasome-mediated degradation. (b) Time-lapse images of a control cell expressing H2B-mCherry and IBB-EGFP, see Supplementary Information, Movie S9. Dashed red line indicates addition of flavopiridol, green bar indicates onset of nuclear IBB-EGFP import. (c) Time-lapse images of a cell transfected with siRNAs targeting PP2A-B55 $\alpha$ , see Supplementary Information, Movie S10. (d, e) Golgi reassembly after chemically-induced mitotic exit. (d) Control cell. (e) Cell transfected with siRNAs targeting PP2A-B55 $\alpha$ . (f, g) Cumulative histograms of nuclear reassembly (f) and Golgi reassembly (g) timing based on the data shown in (b-e). (h) Detection of Cdk1 substrate phosphorylation by an anti-phospho-serine antibody that specifically recognizes the Cdk target sequence (K/R) pS PX (K/R) (pS = phospho-serine) on Western Blot. Samples were prepared after chemical induction of mitotic exit in synchronized cells in presence of proteasome inhibitor as in (a). In control cells, Cdk substrates dephosphorylate rapidly (siControl, lanes 1-7). Cells depleted for PP2A-B55 $\alpha$  show delayed dephosphorylation (lanes 8-14). Scale bars: 10  $\mu$ m.

**Figure 5. Cell cycle-dependent regulation of PP2A-B55 $\alpha$ .** (a) PP2A-B55 $\alpha$  isolated from nocodazole-treated mitotic (M) or unsynchronized interphase cells (I) by pulldown of GST-B55 $\alpha$  was assayed for phosphatase activity towards Cdk1/cyclin B-phosphorylated histone H1 ( $n = 15$ , bars indicate mean; error bars indicate s.d.; \*\* depicts significance by t-test;  $p < 0.001$ ). (b) PP2A-B55 $\alpha$  activity towards substrate phosphorylase a ( $n = 3$ ). (c) Purification of PP2A complexes from interphase (I) or mitotic (M) HeLa cells stably expressing LAP-tagged R1A or B55 $\alpha$  baits. Two mitosis-specific bands were identified by mass spectrometry: Importin  $\beta$ 1 (1), and Importin  $\alpha$ 1 (2). Expected positions of the bands from endogenous PP2A subunits are indicated on the right, migration positions of mouse baits are marked with asterisks. (d) PP2A complexes were purified with R1A-LAP and probed by anti-R1A and anti-Importin  $\beta$ 1 antibodies on a Western Blot. (e) Importin  $\beta$ 1 function in mitotic exit. Cells expressing H2B-mCherry and GalT-EGFP were transfected with siRNAs as indicated. Timing from anaphase ( $t = 0$  min) until Golgi reassembly was assayed as in Fig. 3 ( $n \geq 30$  for each condition). (f) Phosphorylation sites on PP2A-B55 $\alpha$ <sup>34</sup> and in the primary sequence context. The abundance of phosphorylated peptide in the mitotic sample was estimated by peak area quantification of the elution profiles, indicated as percentage of total peptide based on elution profile peak area normalization. Mitotic phosphorylation increase (indicated in brackets) was estimated by comparing the normalized peak area quantifications of phosphorylated peptides in interphase (I) and mitotic (M) samples. (g) B55 $\alpha$ -S167 phosphorylation affects PP2A complex assembly. GST-tagged wildtype-B55 $\alpha$ , non-phosphorylatable S167A, or phospho-mimicking S167E mutants of B55 $\alpha$  were isolated from unsynchronized (I), or mitotic (M) cells by GST-pulldown. PP2A subunits were detected on Western Blots by anti-GST, anti-R1A, and anti-CA antibodies. (h) Model for mitotic exit control. Dephosphorylation of a broad range of mitotic Cdk1 substrates promotes reassembly of interphase cells during mitotic exit. A balance of kinase (Cdk1-Cyclin B) and phosphatase (PP2A-B55 $\alpha$ ) activities determines the substrate dephosphorylation kinetics during mitotic exit. Green indicates activated state, red indicates lower activity, P indicates phosphorylation.

## Online Methods

### Cell lines and plasmids

The HeLa Kyoto cell line was obtained from S. Narumiya, Kyoto University and cultured in DMEM (GIBCO) supplemented with 10% foetal bovine serum (PAA Laboratories) and 1% Penicillin/Streptomycin (Invitrogen). All live imaging experiments were performed using monoclonal reporter cell lines that were generated as described in<sup>35</sup>. For a complete list of plasmids and cell lines see Supplementary Information, Tables 3 and 4. Cells were grown either in 96 well microtiter plates (Greiner), or on LabTek chambered coverslips (Nunc) for live microscopy. Live cell imaging was performed in DMEM containing 10% foetal calf serum and 1% Penicillin/Streptomycin, but without phenolred and riboflavin to reduce autofluorescence of the medium<sup>35</sup>.

The BAC RP24-103C16, harboring mouse PP2A-B55 $\alpha$  (PPP2R2A) as well as BAC RP24-255O20 harboring mouse PPP2CA, were obtained from the BACPAC Resources Center (<http://bacpac.chori.org>). The LAP (EGFP-IRES-Neo)-cassette was PCR amplified using primers that carry 50 nucleotides of homology to the C-terminus of each of the target genes. Recombineering and stable transfection of the modified BAC was performed as described<sup>27</sup>.

### Live cell imaging

Automated microscopy with reflection-based laser autofocus was performed on a Molecular Devices ImageXpressMicro screening microscope equipped with 10x 0.5 N.A. S Fluor dry objective (Nikon), controlled by in-house developed Metamorph macros<sup>21</sup>. Cells were maintained in a microscope stage incubator at 37°C in humidified atmosphere of 5% CO<sub>2</sub> throughout the entire experiment. Illumination was adjusted that cell death rate was below 5% in untreated control cells. Confocal microscopy was performed on a customized Zeiss LSM 510 Axiovert microscope using a 20x 0.8 N.A. Plan-

Apochromat dry, a 40x 1.3 N.A. Oil DIC EC Plan-Neofluar, or 63x 1.4 N.A. Oil Plan-Apochromat objective (Zeiss). The microscope was equipped with piezo focus drives (piezosystemjena), custom-designed filters (Chroma), and EMBL incubation chamber (European Molecular Biology Laboratory), providing a humidified atmosphere at 37°C with 5% CO<sub>2</sub>.

For imaging chemically-induced mitotic exit, cells were seeded in chambered LabTek coverslips overnight and transfected with the respective siRNAs as described above. 52 h post transfection, the medium was replaced with imaging medium containing 30 µM of the proteasome inhibitor MG132 (Sigma). The chambered coverslips were placed to the microscope stage incubator at 37°C in humidified atmosphere of 5% CO<sub>2</sub> for around 45 minutes, during which imaging locations with metaphase arrested cells were selected. These cells were imaged for 10-15 minutes, before mitotic exit was induced with 20 µM of the CDK inhibitor Flavopiridol<sup>25</sup>.

### ***Image analysis and statistical analysis***

Automated image analysis was performed by in house-developed *CellCognition* software<sup>21</sup> (<http://www.cellcognition.org>). Cell nuclei and mitotic chromosome masses were detected by local adaptive thresholding. Cytoplasmic regions were derived by region growing of the chromatin segmentation to a fixed size. Next, texture and shape features were calculated for each object and samples for mitotic classes were manually annotated for supervised classification. Support vector machine classification was by radial-based kernel and probability estimates. Tracking cells over time was by a constrained nearest-neighbour, with an algorithm that supported trajectory splitting and merging. Mitotic events were detected in the graph structure based on the transition from prophase to prometaphase. Increase of the nuclear/cytoplasmic ratio of mean IBB-mEGFP fluorescence >1.5-fold above the ratio at the time point of chromosome segregation defined the state with nuclear envelope assembled. In the RNAi screen, mean mitotic exit timing was normalized per 96-well plate to compensate slight differences in the temporal sampling rate. Z-scores were calculated based on the mean and standard deviation of all data points. All statistical testing was by two-tailed Student's t-test.

### ***RNAi***

The human siRNA phosphatase library was based on version V3.0 from Qiagen and complemented with custom siRNAs targeting missing phosphatases. For a complete list of siRNA oligos see Supplementary Information, Tables 1 and 2. RNAi duplexes were transfected in liquid phase with either Oligofectamine (Invitrogen) or HiPerfect (Qiagen) according to the manufacturer's protocols. Final siRNA concentrations were 50 nM for Oligofectamine or 10 nM for HiPerfect. Cells were reversely transfected in 96 well microtiter plates and incubated for about 40 h before imaging.

### ***Quantitative real time PCR***

mRNA was extracted from cells 40 h after transfection of siRNAs, using the TurboCapture 8 mRNA Kit (Qiagen), cDNA was prepared using random hexamer primers (Microsynth) and Ready-to-go you-prime first-strand beads (GE Healthcare). Real time PCR was performed using LightCycler 480 SYBR Green I Master (Roche Diagnostics). Primers were designed using AutoPrime ([www.autoprime.de](http://www.autoprime.de)) or Clone Manager. Primer pairs were: *CA* (5'-GGAGCTGGTTACACCTTG-3', 5'-CCAGTTATATCCCTCCATCAC-3'), *R1A* (5'-CTTCAATGTGGCCAAGTCTC-3', 5'-TCTAGGATGGGCTTGACTTC-3') *B55α* (5'-ATTCGGCTATGTGACATGAG-3', 5'-GACCTGTTACTGGGATCTC-3'), *B55δ* (5'-CTG AAAGACGAAGATGGAAG-3', 5'-AATATTGGGACCCGTAGC-3'), *Importin β1* (5'- CAGATACG AGGGTACGAGTG-3', 5'-TTTCATTGCTCGATTGTG-3'), *GAPDH* (5'-CGTGTCAAGTGGGACCTGACC-3', 5'-CTGCTTCACCACCTTCTTGATGTCA-3').

### ***Protein blotting***

Pelleted cells were washed with PBS and total protein lysates prepared in lysis buffer (50 mM Tris, pH 7.5, 150 mM NaCl, 1% Nonidet P-40, 10% glycerol, 2 mM EDTA), supplemented with Mini-Complete protease inhibitor tablet (Roche), and 20 mM beta-glycerophosphate. Protein concentrations were determined using a BCA kit (Pierce). The following primary antibodies were used: polyclonal rabbit-anti-PPP2CA (1:2,000 dilution, Cell Signaling), polyclonal rabbit-anti-PPP2R1A (1:2,000 dilution, Cell Signaling), monoclonal mouse-anti-PP2A-B55-alpha (1:500 dilution, Santa Cruz), polyclonal rabbit-anti-phospho-(Ser) CDKs substrate (1:1,000 dilution, Cell Signaling), monoclonal mouse-anti-CyclinB1 (1:5,000 dilution, Santa Cruz), monoclonal mouse-anti-Actin (1:50,000 dilution, Millipore).

For the chemically-induced mitotic exit assay, nocodazole arrested cells (100 ng/ml for 17 h; Sigma) were incubated for 30 min in 30 µM of MG132 (Sigma), collected by shake-off, washed in PBS containing MG132, resuspended in 800 µl of PBS (+MG132), and 100 µl of this suspension was aliquoted in 1.5 ml centrifugation tubes and kept at 37°C. Mitotic exit was induced by adding flavopiridol to 20 µM (provided by the National Cancer Institute with permission by Sanofi Aventis). Cell aliquots were lysed at 3 minute intervals over a time period of 18 minutes, by adding 5x concentrated SDS cracking buffer to the respective aliquot, and boiling it for 5 minutes at 95°C. Quantitative Western blotting was performed using the LICOR Odyssey system or with the FluorChem system from Alpha Innotec.

### ***Immunoprecipitation and GST pull downs***

Immunoprecipitations of HA-CA-transfected HeLa Kyoto cells were performed as described<sup>31</sup>. HA-CA complexes were subjected to Western blotting with monoclonal mouse anti-C and anti-A (1:2,000, Dr. S. Dilworth), and polyclonal rabbit anti-B55α antibodies (1:500, Calbiochem).

Subconfluent HeLa Kyoto cells expressing GST-B55α were untreated (I) or mitotically arrested with nocodazole (100 ng/ml for 16 h) (M). Following collection by scraping (I) or shake off (M), cells were washed in PBS, pooled and lysed in 1 ml NET buffer (50 mM Tris, pH 7.4, 150 mM NaCl, 1% Nonidet P-40, 15 mM EDTA), supplemented with Mini-Complete protease inhibitors (Roche) and, when appropriate, with phosphatase inhibitor tablet (Roche). Equal amounts of the cleared lysates (as measured by BCA (Pierce)) were added to 25 µl Glutathione-Sepharose (GE Healthcare) and allowed to bind for 1h at 4°C. As previously shown<sup>31</sup>, this method allows isolation of catalytically competent PP2A-B55α trimers. After 4 washes inNET-100<sup>31</sup> and 1 wash in PP2A assay buffer (20 mM Tris pH 7.4, 5 mM DTT), assay buffer was added to the beads for phosphatase assays on two different substrates (histone H1, phosphorylase *a*) for at least two time points and with three replicas for each measurement (final volume 100-120 µl). A small aliquot was used for Western blotting with anti-C and anti-A (monoclonals Dr. S. Dilworth, 1:2,000) and anti-GST antibodies (Sigma, 1:10,000) to double-check for equal input.

### ***Phosphatase assays***

6 µg of histone H1 (Roche) were phosphorylated with Cdk1/cyclin B1 (Biaffin) or Cdk2/cyclin A<sup>36</sup> in the presence of [<sup>32</sup>P]-ATP (GE Healthcare) to a level of 5-7 moles/mole. [<sup>32</sup>P]radiolabelled histone H1 was precipitated in 25% trichloroacetic acid (TCA), washed twice in 25% TCA, once in acetone/HCl (200:1) and once in acetone. This pellet was solubilised in PP2A assay buffer and used at 0.3 µM. Following different incubation times with PP2A-B55α at 30°C (2, 5, 10 or 20 minutes), release of inorganic [<sup>32</sup>P]-phosphate was measured through extraction of a phospho-molybdate complex and scintillation counting<sup>37</sup>. Under these conditions phosphate release was <10% of the phosphorylated substrate and thus remained in the linear range. Phosphorylase *a* phosphatase assays were performed as described<sup>38</sup>, by measuring the liberated TCA soluble [<sup>32</sup>P]-phosphate following a 10- or 20-minute incubation with PP2A-B55α. Each measurement of phosphatase activity was in triplicate. PP2A-B55α activities from mitotic cells were normalized to PP2A-B55α activities from interphase cells.

### ***Affinity purification of protein complexes***

HeLa cell pools expressing LAP-tagged mouse PP2A subunits in bacterial artificial chromosomes (BACs) were cultured in ten 25-cm square tissue culture trays. Cells were harvested from two culture conditions: prometaphase arrest induced by incubation in  $0.1 \mu\text{g ml}^{-1}$  nocodazole for 18 hr; and during exponential ('log-phase') growth, yielding cells typically >90% in interphase. PP2A complexes were isolated from concentrated extracts of these cells, using the two-step purification procedure previously described<sup>27</sup>, except that okadaic acid was included the extract buffer and all subsequent solutions, to restrain auto-dephosphorylation. 20% of the purified protein complex was analysed by SDS-PAGE and silver staining; the remaining sample was processed as described<sup>39</sup>, then divided into two aliquots for parallel in-solution digestion by trypsin and subtilisin, then analysis by liquid chromatography - mass spectrometry (MS) for protein identification and phosphorylation site mapping.

### ***Trypsin digestion of SDS-PAGE gel slices***

Selected silver-stained protein bands were excised from an SDS-PAGE gel, cut into smaller pieces and washed by incubating in a shaking incubator once with 200  $\mu\text{l}$  of 50 mM triethyl ammonium bicarbonate (TEAB), then once with 100  $\mu\text{l}$  acetonitrile (ACN) plus 100  $\mu\text{l}$  of 50 mM TEAB. Each wash step was performed in a shaking incubator at room temperature. This two-step wash procedure was repeated once, and then excess liquid removed. To shrink the gel pieces, 100  $\mu\text{l}$  ACN was added to them.

Proteins were reduced by incubating the gel pieces in 100  $\mu\text{l}$  of 1 mg  $\text{ml}^{-1}$  dithiothreitol in 50 mM TEAB at 57°C for 30 min, then excess liquid was removed. Proteins were alkylated by incubating the gel pieces with 100  $\mu\text{l}$  of 5 mg  $\text{ml}^{-1}$  iodacetamide in 50 mM TEAB at room temperature, in the dark, for 35 min. Gel pieces were subjected to the two-step wash and shrinking procedures as previously described, and were then centrifuged in a vacuum concentrator (SpeedVac, Thermo Scientific) until dry (5-7 min).

Trypsin Gold (Promega) was first dissolved in 100 ng  $\mu\text{l}^{-1}$  in 50 mM acetic acid, then diluted in 50 mM TEAB to a concentration of 12 ng  $\mu\text{l}^{-1}$ . Gel pieces were incubated with 20  $\mu\text{l}$  trypsin/TEAB solution at 4°C for 5 min. Excess liquid was removed, and 20  $\mu\text{l}$  of 50 mM TEAB was added, followed by incubation at 37°C overnight. After centrifugation, the supernatant was transferred into a fresh tube and stored at 5°C. 20  $\mu\text{l}$  of 5% formic acid was added to the gel pieces, followed by sonication for 10 min in a cooled ultrasonic waterbath. The sample was spun and the supernatant transferred to the tube as mentioned previously. This formic acid / sonication step was repeated once, and the supernatant pooled with the first, generating a sample of volume 60  $\mu\text{l}$ , ready for analysis by MS.

### ***NanoLC-MS***

The nano HPLC system used in all experiments was an UltiMate 3000 Dual Gradient HPLC system (Dionex, Amsterdam, The Netherlands), equipped with a Proxeon nanospray source (Proxeon, Odense, Denmark), coupled to an LTQ-FT mass spectrometer (Thermo Fisher Scientific, Bremen, Germany) in the first analysis and coupled to an LTQ Velos Orbitrap mass spectrometer (Thermo Fisher Scientific) in the second analysis. The LTQ FT was operated in data-dependent mode using a full scan in the ICR cell followed by MS/ MS scans of the five most abundant ions in the linear ion trap. MS/MS spectra were acquired in the multistage activation mode, where subsequent activation was performed on fragment ions resulting from the neutral loss of -98, -49, or -32.6 m/z. Precursor ions selected for fragmentation were put on a dynamic exclusion list for 180 s. Monoisotopic precursor selection was enabled. Phosphopeptides identified by database search and validated by manual inspection were put onto an inclusion list and replicate analyses were carried out on an LTQ Velos Orbitrap mass spectrometer.

### ***Analysis of MS data***

For peptide identification, all MS/MS spectra were searched using Mascot 2.2.0 (Matrix Science, London, UK) against a customised protein sequence database comprising the complete human

sequences from Swiss-Prot, TrEMBL, PIR, GenBank, EMBL, DDBJ, RefSeq and Celera (hKBMS), plus the Swiss-Prot entries corresponding to the mouse ‘bait’ proteins. The following search parameters were used: carbamidomethylation on cysteine was set as a fixed modification, oxidation on methionine, phosphorylation on serine, threonine and tyrosine was set as variable modifications. Monoisotopic masses were searched within unrestricted protein masses for tryptic peptides. The peptide mass tolerance was set to  $\pm 5$  ppm and the fragment mass tolerance to  $\pm 0.5$  Da. The maximal number of missed cleavages was set to 2. Each MS/MS spectrum corresponding to a predicted phosphopeptide was validated by visual inspection. A label-free quantification approach was used to determine abundance change from interphase (log) to mitosis (noc) of the different peptides by peak area integration. For peak area quantification we extracted the ion chromatograms of the peptides with a mass tolerance of 3 ppm using the Qual Browser application from the Xcalibur software package. The mass traces of peak area integration for the phosphopeptides shown in Fig. 5f were extracted from the base peak chromatogram with  $\pm 3$  ppm mass tolerance, manually reviewed and are shown in Supplementary Information, Fig. S8.

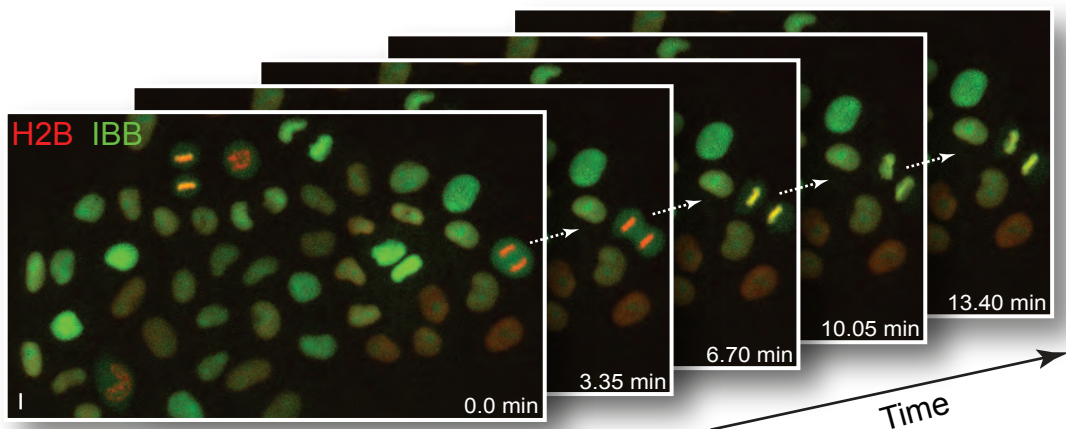
## References

1. Morgan, D.O. *The cell cycle: principles of control*. (Oxford University Press, NSP, 2007).
2. Queralt, E. & Uhlmann, F. Cdk-counteracting phosphatases unlock mitotic exit. *Curr Opin Cell Biol* **20**, 661-668 (2008).
3. Bollen, M., Gerlich, D.W. & Lesage, B. Mitotic phosphatases: from entry guards to exit guides. *Trends Cell Biol* (2009).
4. Trinkle-Mulcahy, L. & Lamond, A.I. Mitotic phosphatases: no longer silent partners. *Curr Opin Cell Biol* **18**, 623-631 (2006).
5. Wu, J.Q. *et al.* PP1-mediated dephosphorylation of phosphoproteins at mitotic exit is controlled by inhibitor-1 and PP1 phosphorylation. *Nat Cell Biol* **11**, 644-651 (2009).
6. Mochida, S., Ikeo, S., Gannon, J. & Hunt, T. Regulated activity of PP2A-B55delta is crucial for controlling entry into and exit from mitosis in Xenopus egg extracts. *EMBO J* **28**, 2777-2785 (2009).
7. Stegmeier, F. & Amon, A. Closing mitosis: the functions of the Cdc14 phosphatase and its regulation. *Annu Rev Genet* **38**, 203-232 (2004).
8. Berdugo, E., Nachury, M.V., Jackson, P.K. & Jallepalli, P.V. The nucleolar phosphatase Cdc14B is dispensable for chromosome segregation and mitotic exit in human cells. *Cell Cycle* **7**, 1184-1190 (2008).
9. Gruneberg, U., Glotzer, M., Gartner, A. & Nigg, E.A. The CeCDC-14 phosphatase is required for cytokinesis in the *Caenorhabditis elegans* embryo. *J Cell Biol* **158**, 901-914 (2002).
10. Mailand, N. *et al.* Derepressed human Cdc14A phosphatase disrupts centrosome separation and chromosome segregation. *Nat Cell Biol* **4**, 317-322 (2002).
11. Mocciaro, A. *et al.* Vertebrate cells genetically deficient for Cdc14A or Cdc14B retain DNA damage checkpoint proficiency but are impaired in DNA repair. *J Cell Biol* **189**, 631-639 (2010).
12. Nishiyama, T., Yoshizaki, N., Kishimoto, T. & Ohsumi, K. Transient activation of calcineurin is essential to initiate embryonic development in *Xenopus laevis*. *Nature* **449**, 341-345 (2007).
13. Mochida, S. & Hunt, T. Calcineurin is required to release Xenopus egg extracts from meiotic M phase. *Nature* **449**, 336-340 (2007).
14. Mayer-Jaekel, R.E. *et al.* The 55 kd regulatory subunit of Drosophila protein phosphatase 2A is required for anaphase. *Cell* **72**, 621-633 (1993).
15. Axton, J.M., Dombradi, V., Cohen, P.T. & Glover, D.M. One of the protein phosphatase 1 isoforms in Drosophila is essential for mitosis. *Cell* **63**, 33-46 (1990).
16. Doonan, J.H. & Morris, N.R. The bimG gene of *Aspergillus nidulans*, required for completion of anaphase, encodes a homolog of mammalian phosphoprotein phosphatase 1. *Cell* **57**, 987-996 (1989).
17. Janssens, V., Longin, S. & Goris, J. PP2A holoenzyme assembly: in cauda venenum (the sting is in the tail). *Trends Biochem Sci* **33**, 113-121 (2008).
18. Neumann, B. *et al.* Phenotypic profiling of the human genome by time-lapse microscopy reveals cell division genes. *Nature* **464**, 721-727 (2010).
19. Steigemann, P. *et al.* Aurora B-mediated abscission checkpoint protects against tetraploidization. *Cell* **136**, 473-484 (2009).
20. Dultz, E. *et al.* Systematic kinetic analysis of mitotic dis- and reassembly of the nuclear pore in living cells. *J Cell Biol* **180**, 857-865 (2008).
21. Held, M. *et al.* CellCognition: time-resolved phenotype annotation in high-throughput live cell imaging. *Nature Methods* **In press** (2010).
22. Schaub, B.E., Berger, B., Berger, E.G. & Rohrer, J. Transition of galactosyltransferase 1 from trans-Golgi cisterna to the trans-Golgi network is signal mediated. *Mol Biol Cell* **17**, 5153-5162 (2006).
23. Leonhardt, H. *et al.* Dynamics of DNA replication factories in living cells. *J Cell Biol* **149**, 271-280. (2000).
24. Lee, T.H., Turck, C. & Kirschner, M.W. Inhibition of cdc2 activation by INH/PP2A. *Mol Biol Cell* **5**, 323-338 (1994).

25. Potapova, T.A. *et al.* The reversibility of mitotic exit in vertebrate cells. *Nature* **440**, 954-958 (2006).
26. Skoufias, D.A., Indorato, R.L., Lacroix, F., Panopoulos, A. & Margolis, R.L. Mitosis persists in the absence of Cdk1 activity when proteolysis or protein phosphatase activity is suppressed. *J Cell Biol* **179**, 671-685 (2007).
27. Poser, I. *et al.* BAC TransgeneOmics: a high-throughput method for exploration of protein function in mammals. *Nat Methods* **5**, 409-415 (2008).
28. Harel, A. & Forbes, D.J. Importin beta: conducting a much larger cellular symphony. *Mol Cell* **16**, 319-330 (2004).
29. Guo, H. & Damuni, Z. Autophosphorylation-activated protein kinase phosphorylates and inactivates protein phosphatase 2A. *Proc Natl Acad Sci U S A* **90**, 2500-2504 (1993).
30. Mayer-Jaekel, R.E. *et al.* Drosophila mutants in the 55 kDa regulatory subunit of protein phosphatase 2A show strongly reduced ability to dephosphorylate substrates of p34cdc2. *J Cell Sci* **107 ( Pt 9)**, 2609-2616 (1994).
31. Longin, S. *et al.* Selection of protein phosphatase 2A regulatory subunits is mediated by the C terminus of the catalytic Subunit. *J Biol Chem* **282**, 26971-26980 (2007).
32. Shi, Y. Serine/threonine phosphatases: mechanism through structure. *Cell* **139**, 468-484 (2009).
33. Huang, H.C., Shi, J., Orth, J.D. & Mitchison, T.J. Evidence that mitotic exit is a better cancer therapeutic target than spindle assembly. *Cancer Cell* **16**, 347-358 (2009).
34. Xu, Y., Chen, Y., Zhang, P., Jeffrey, P.D. & Shi, Y. Structure of a protein phosphatase 2A holoenzyme: insights into B55-mediated Tau dephosphorylation. *Mol Cell* **31**, 873-885 (2008).
35. Schmitz, M.H. & Gerlich, D.W. Automated live microscopy to study mitotic gene function in fluorescent reporter cell lines. *Methods Mol Biol* **545**, 113-134 (2009).
36. Amniai, L. *et al.* Alzheimer disease specific phosphoepitopes of Tau interfere with assembly of tubulin but not binding to microtubules. *FASEB J* **23**, 1146-1152 (2009).
37. Shacter-Noiman, E. & Chock, P.B. Properties of a Mr = 38,000 phosphoprotein phosphatase. Modulation by divalent cations, ATP, and fluoride. *J Biol Chem* **258**, 4214-4219 (1983).
38. Waelkens, E., Goris, J. & Merlevede, W. Purification and properties of polycation-stimulated phosphorylase phosphatases from rabbit skeletal muscle. *J Biol Chem* **262**, 1049-1059 (1987).
39. Gregan, J. *et al.* Tandem affinity purification of functional TAP-tagged proteins from human cells. *Nat Protoc* **2**, 1145-1151 (2007).
40. Mitulovic, G. *et al.* Automated, on-line two-dimensional nano liquid chromatography tandem mass spectrometry for rapid analysis of complex protein digests. *Proteomics* **4**, 2545-2557 (2004).

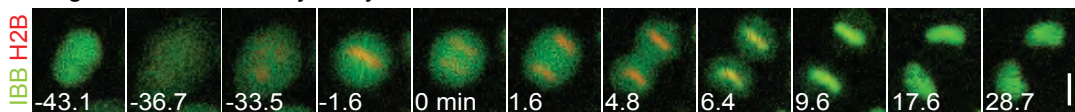
# Figure 1

a



b

Original data of cell trajectory



c

Supervised machine learning & classification



d

Nucleo-cytoplasmic ratio measurements

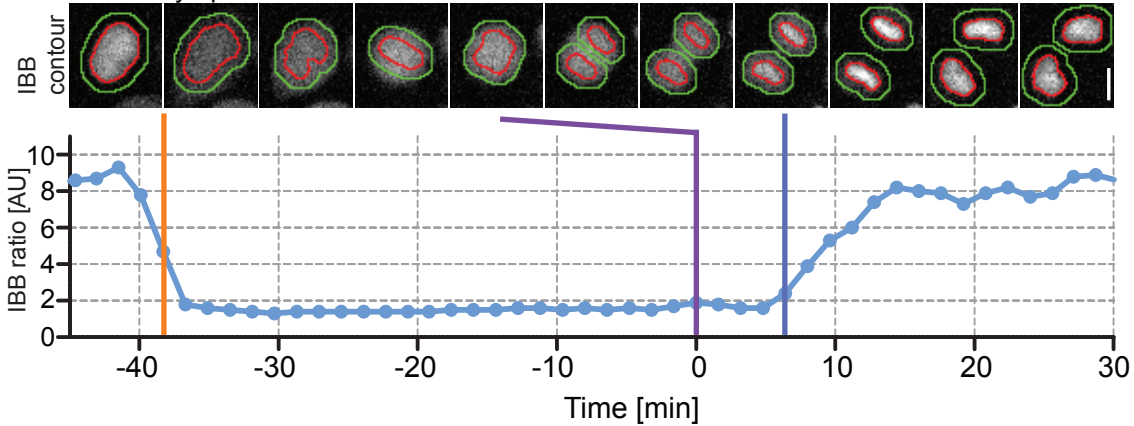


## Figure 2

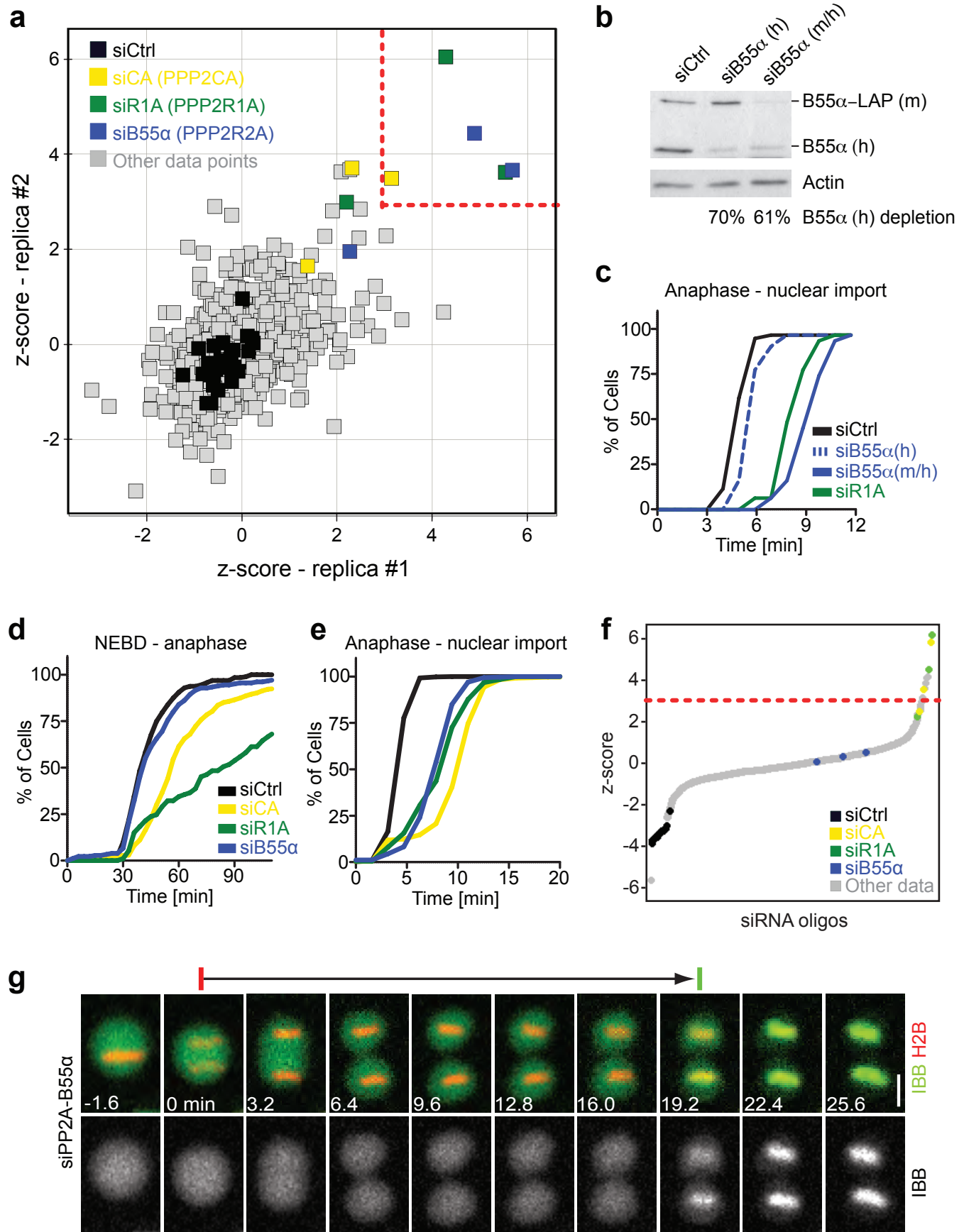


**Figure 3**

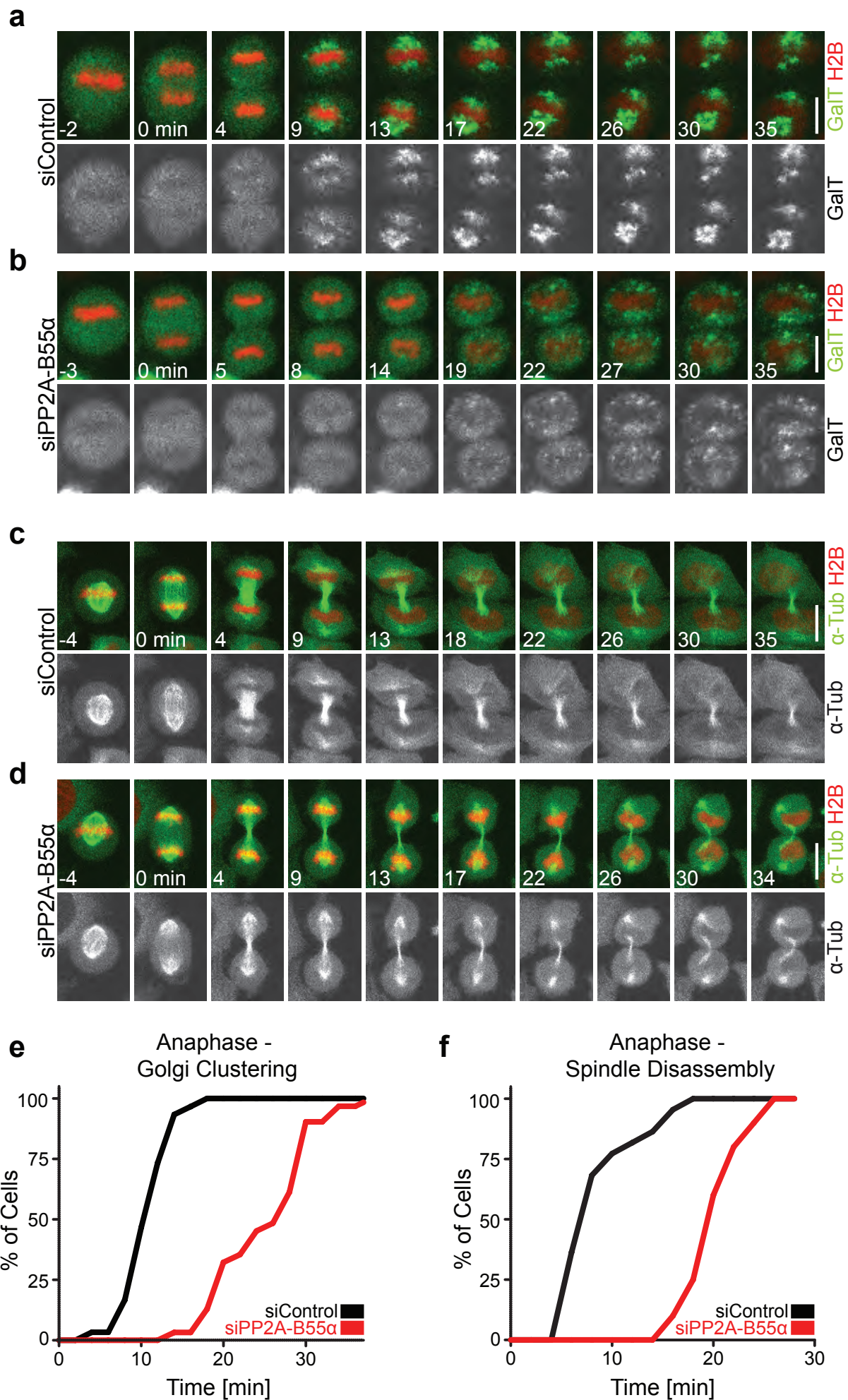


# Figure 4

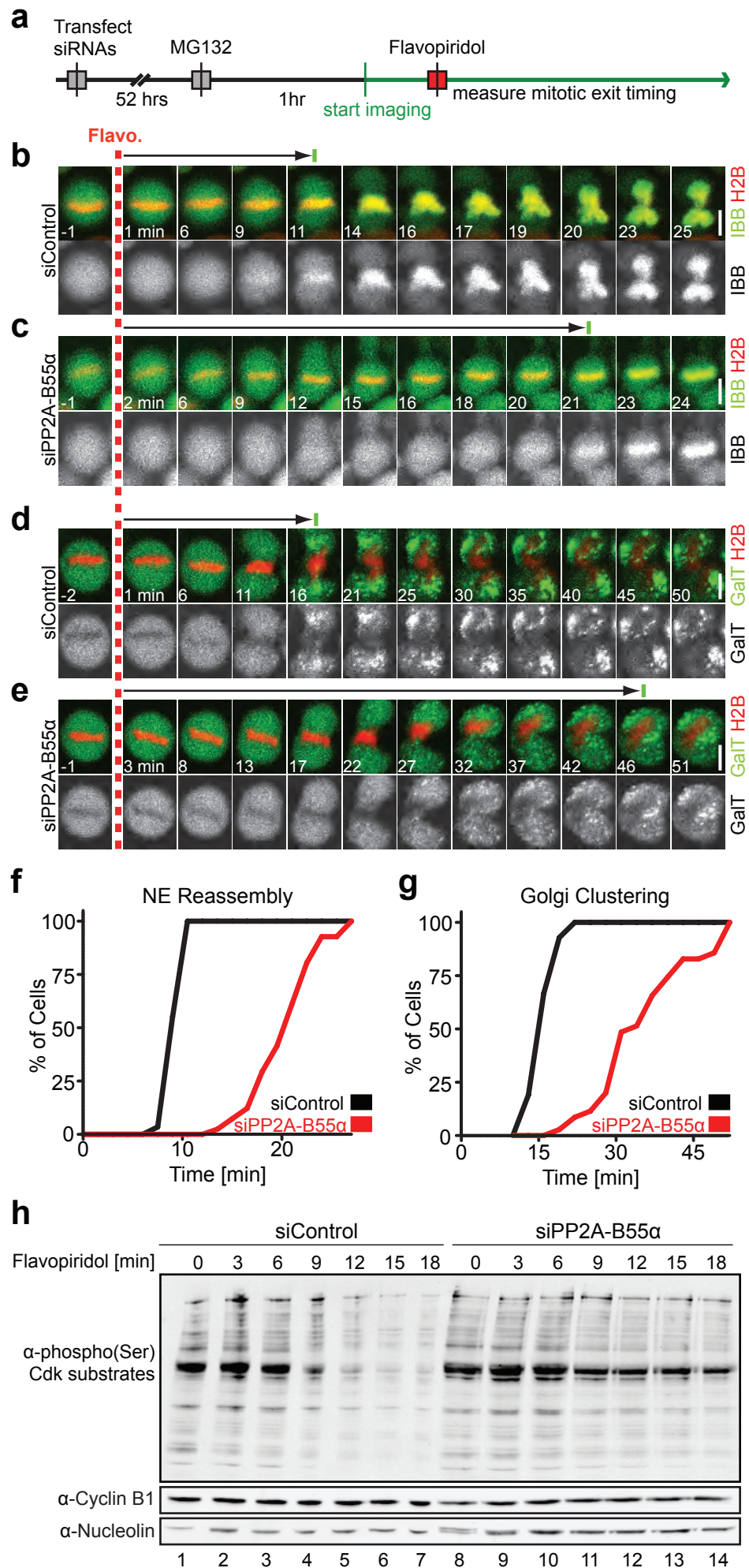
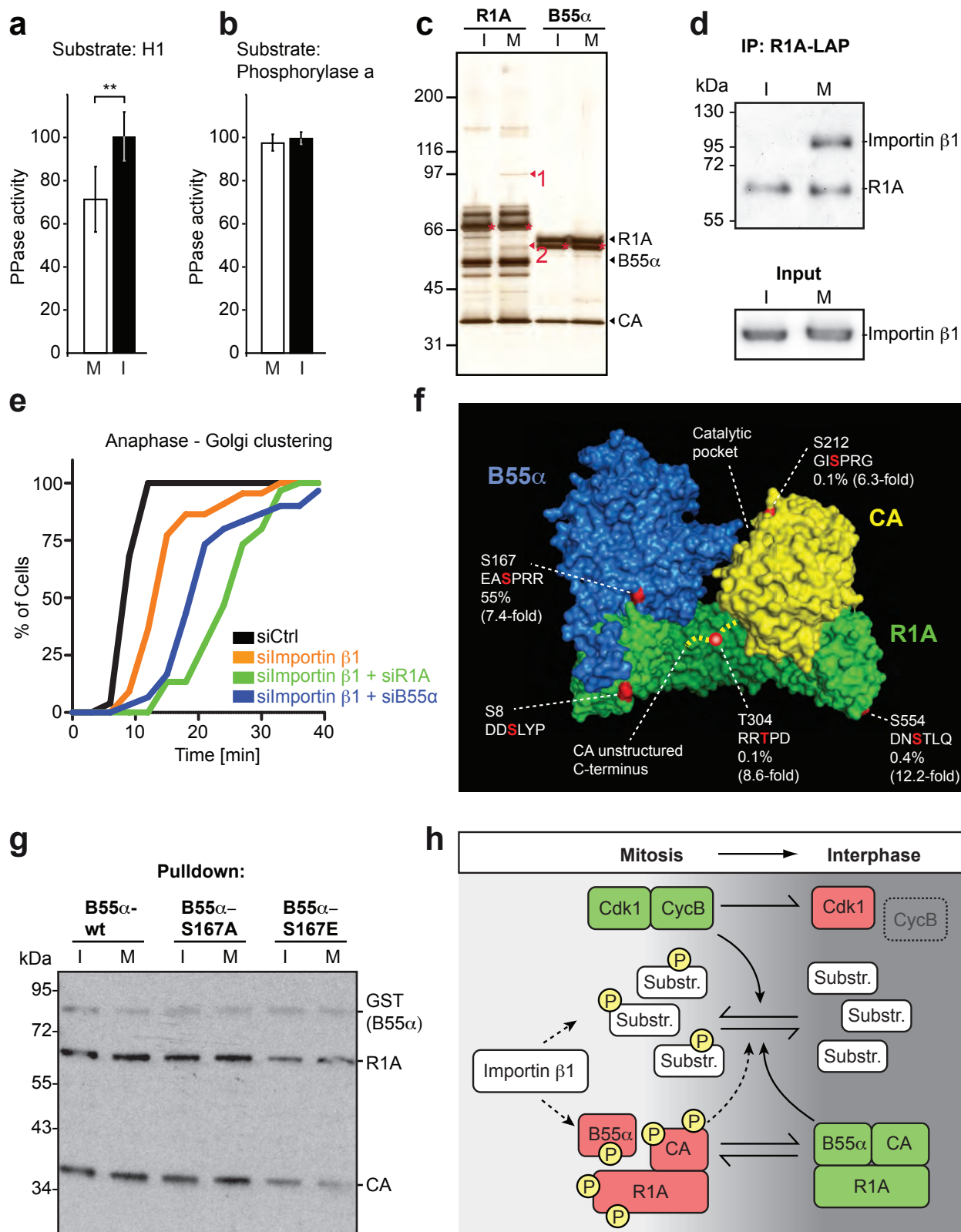
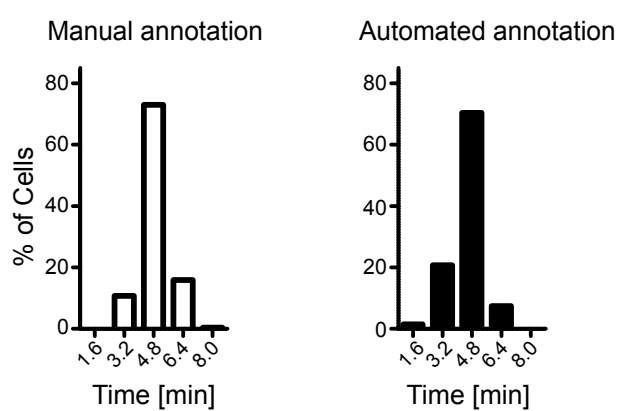


# Figure 5

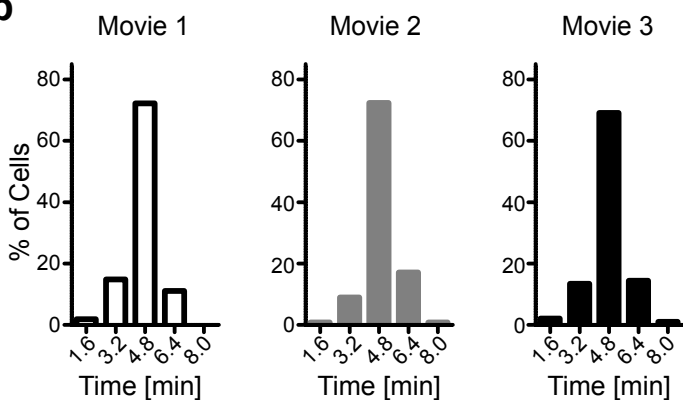


## Supplementary Information, Figure S1

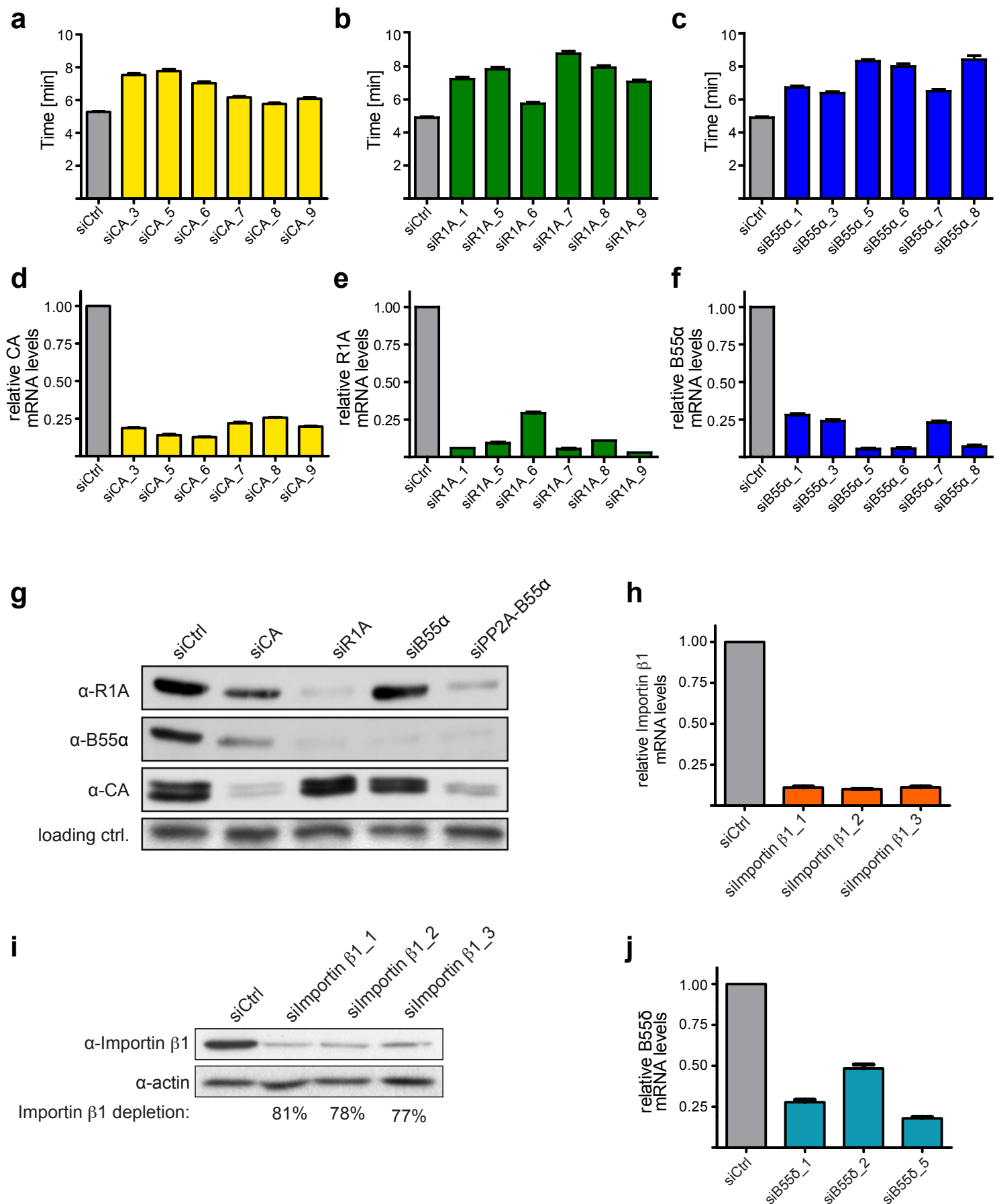
**a**



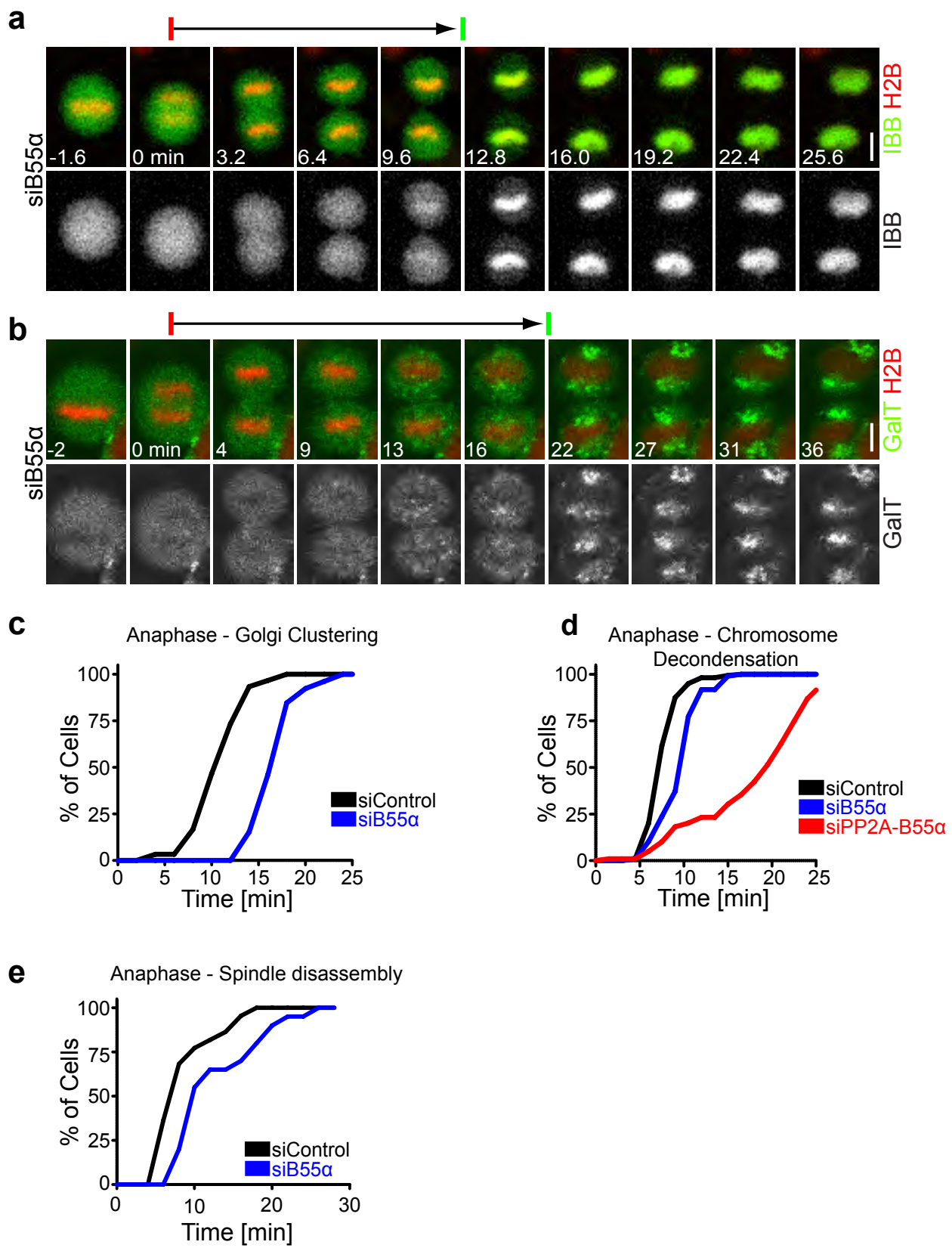
**b**



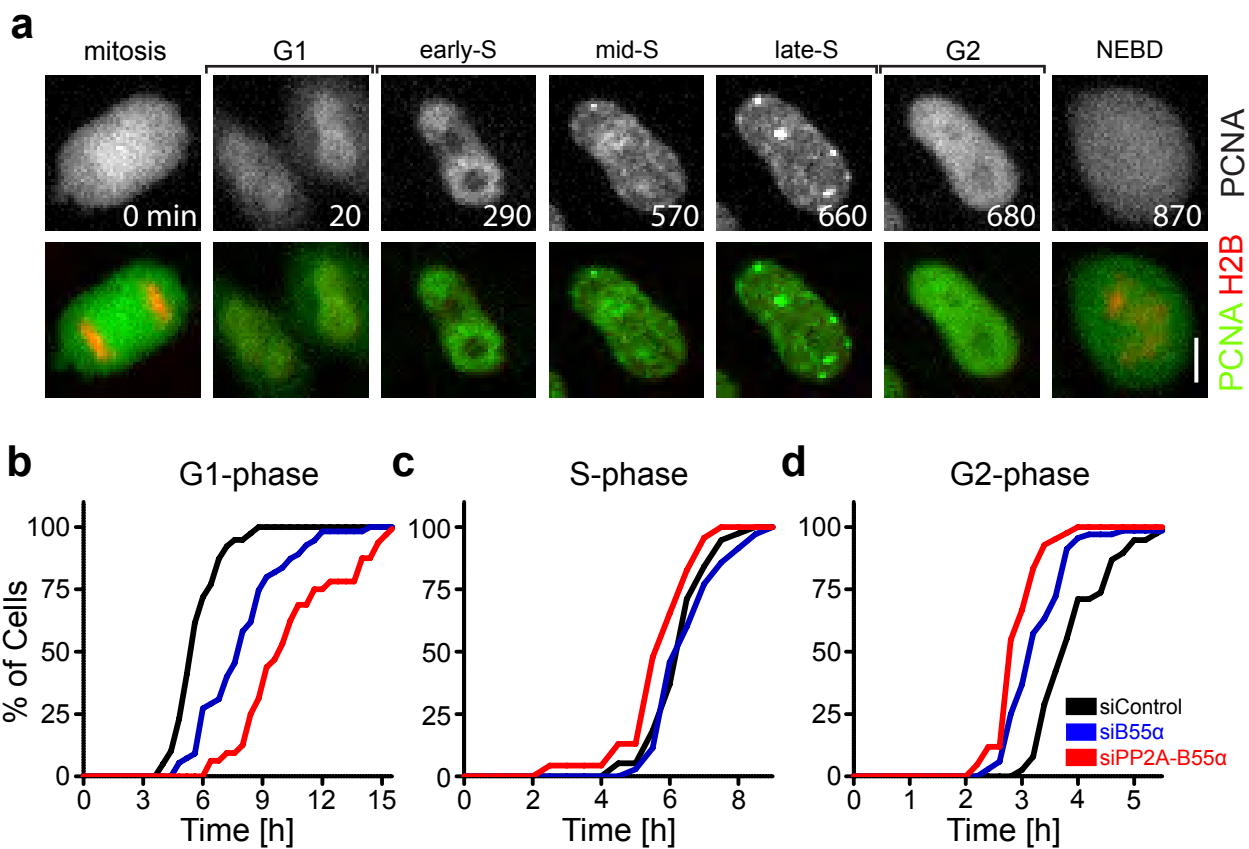
## Supplementary Information, Figure S2



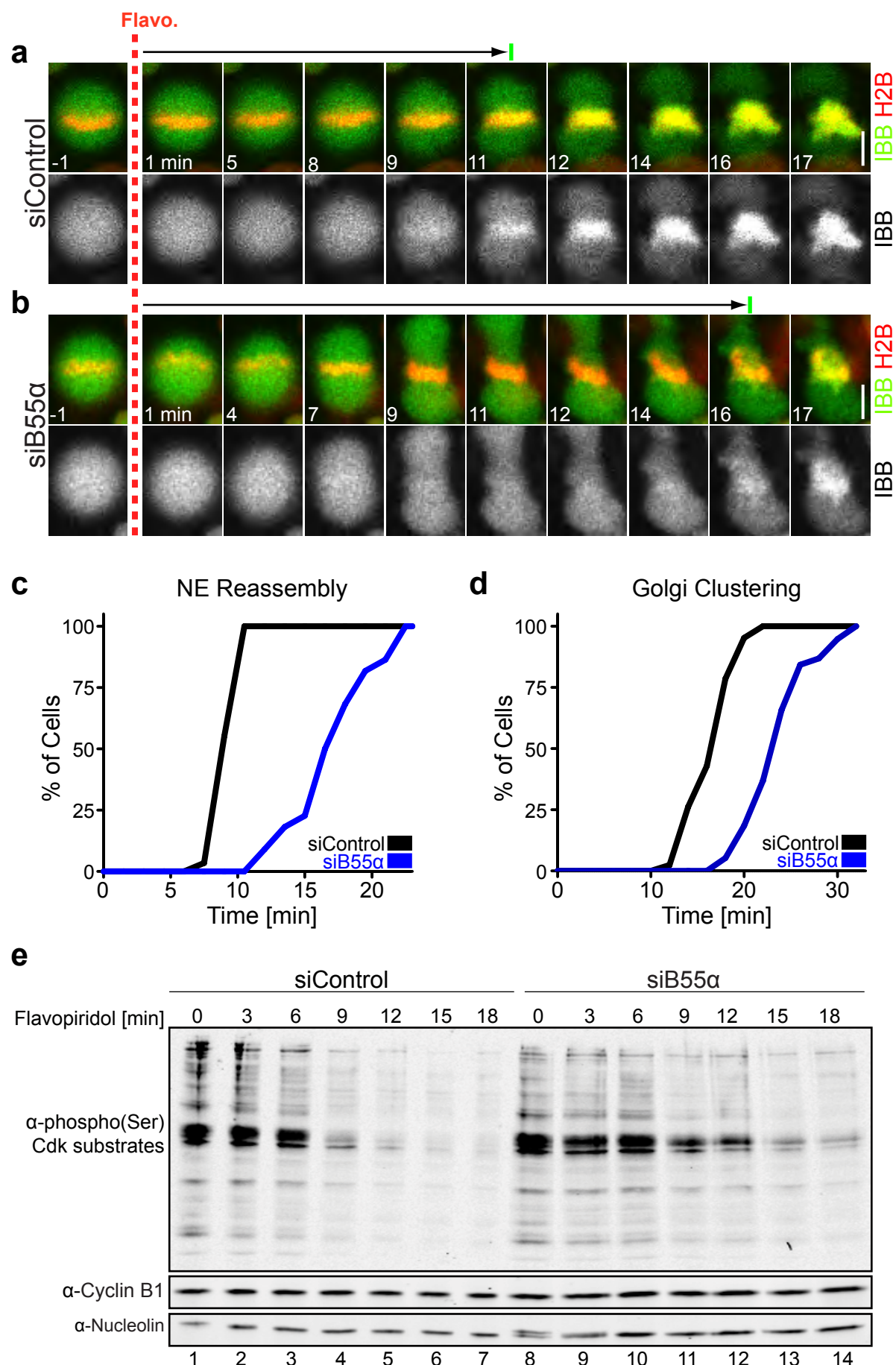
## Supplementary Information, Figure S3



## Supplementary Information, Figure S4

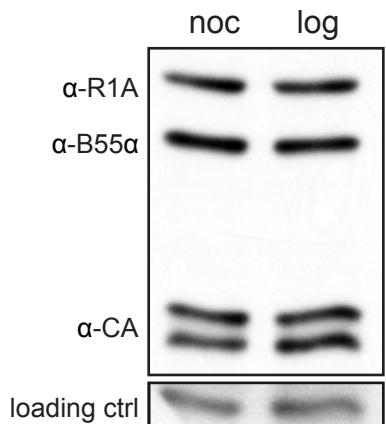


## Supplementary Information, Figure S5

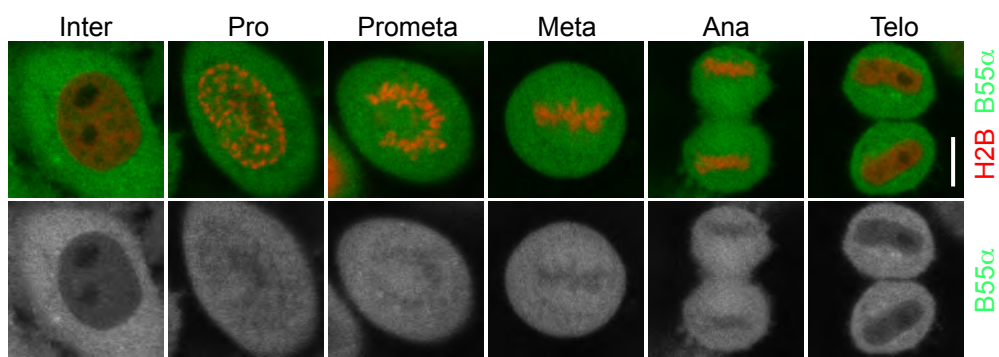


## Supplementary Figure S6

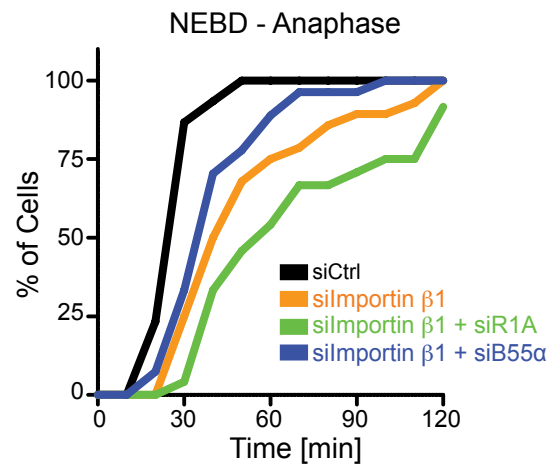
**a**



**b**

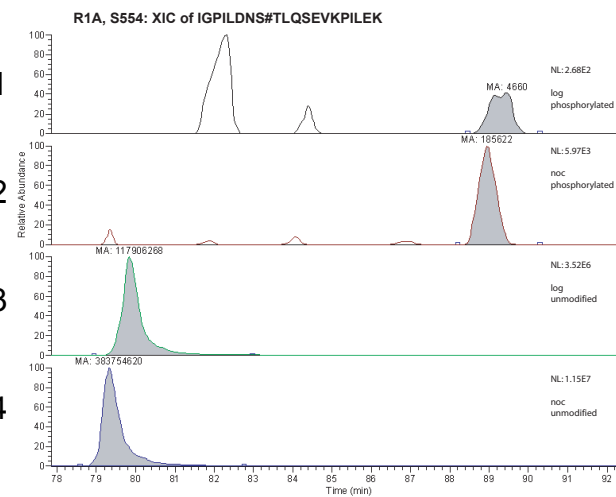


## Supplementary Information, Figure S7



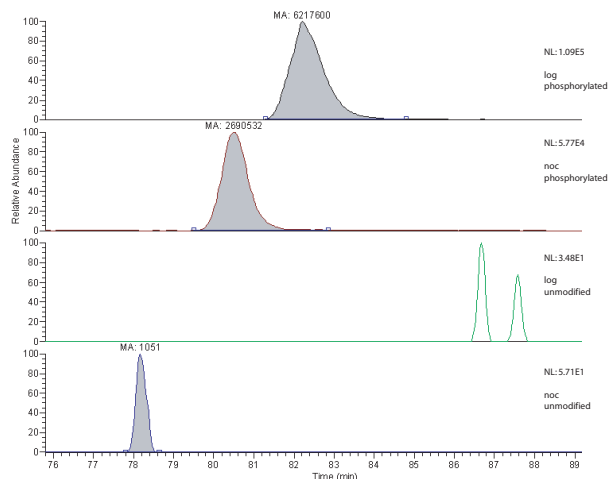
# Supplementary Information, Figure S8

**a**

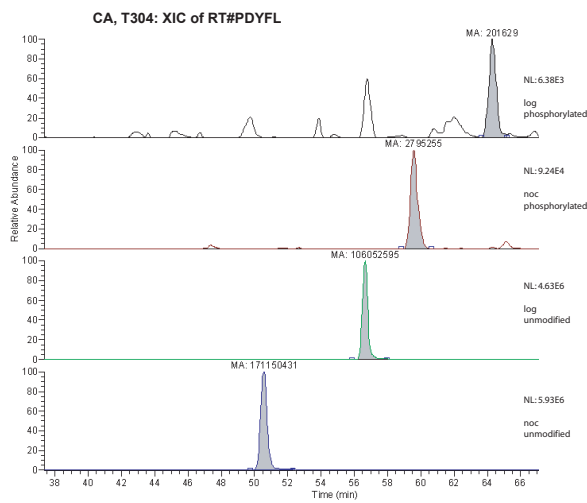


**b**

R1A, S8: XIC of AAADGDDDS#LYPIA

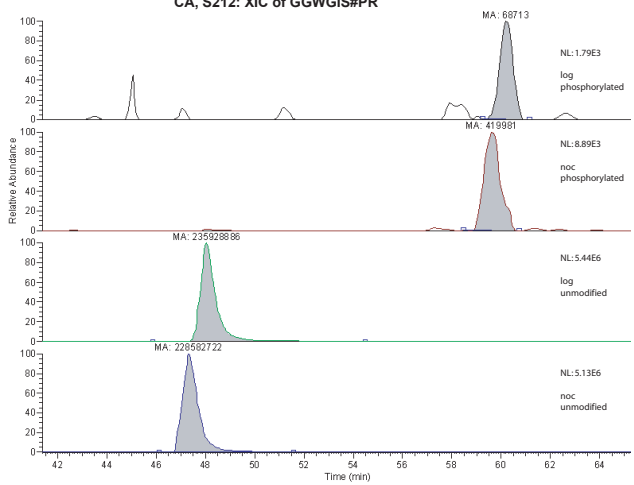


**c**



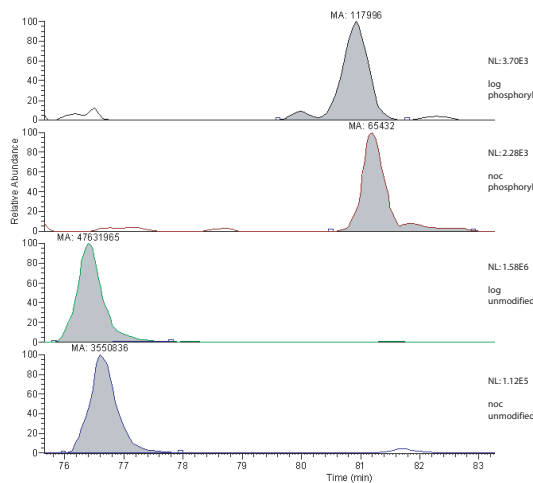
**d**

CA, S212: XIC of GGWGGS#PR



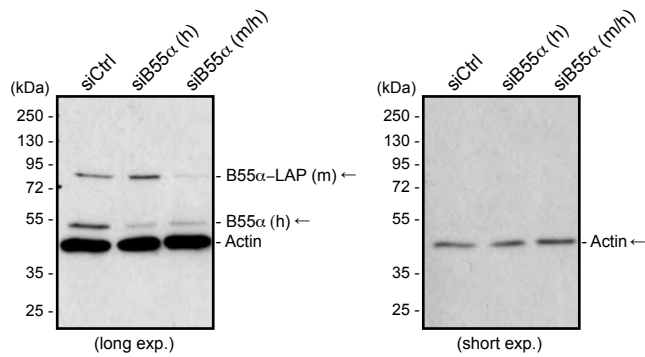
**e**

B55a, S167: XIC of VPVFRPMDLMEAS#PR

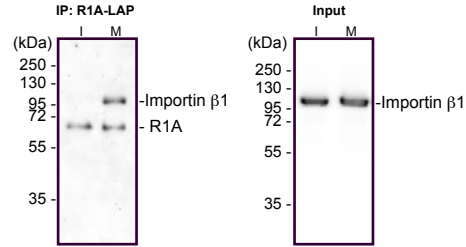


# Supplemental Figure S9

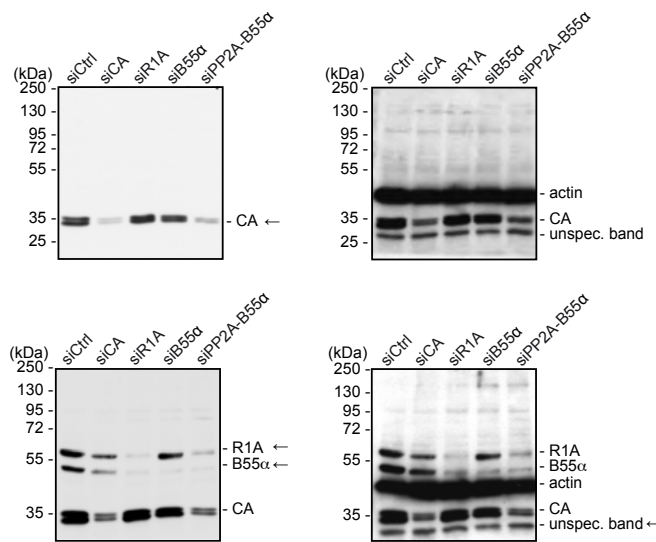
**a**



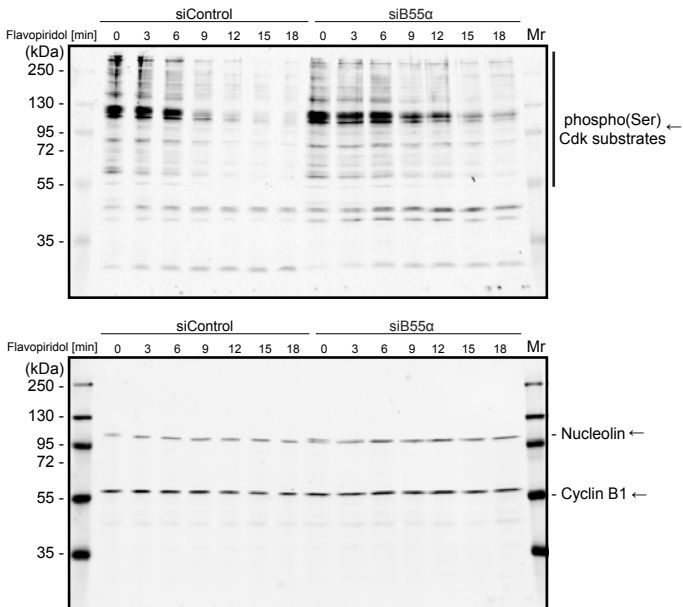
**c**



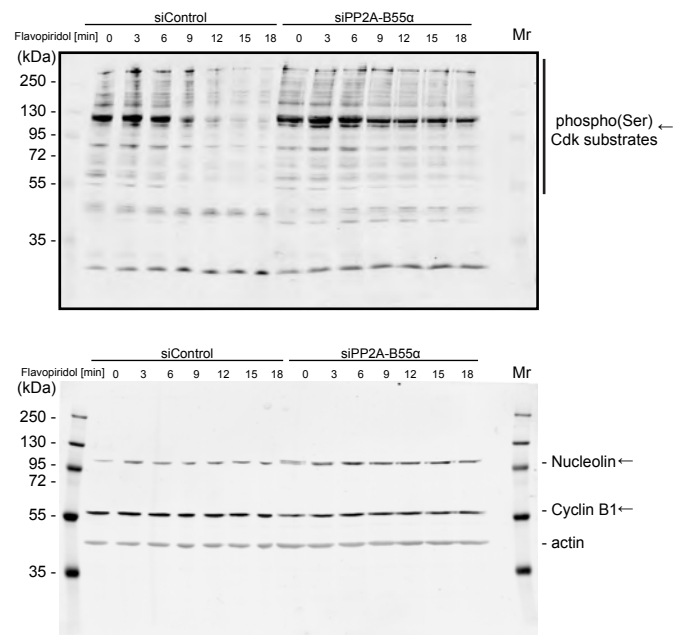
**d**



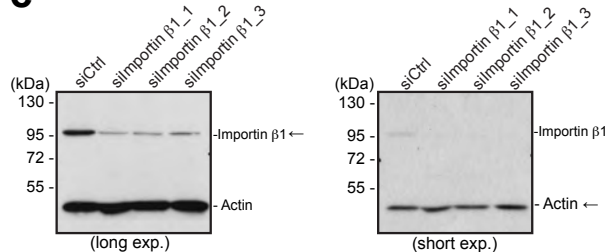
**f**



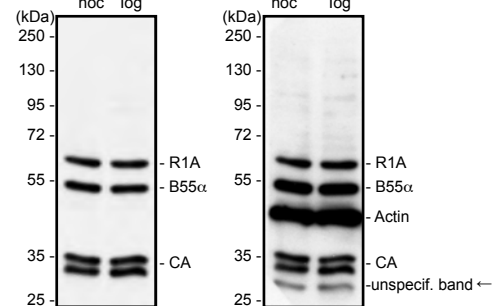
**b**



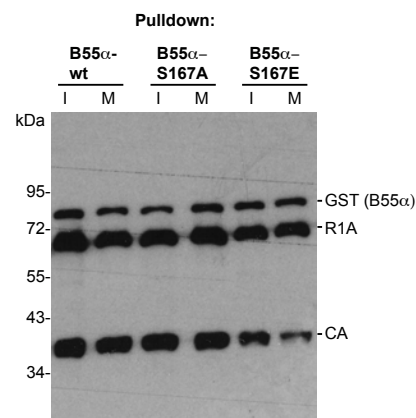
**e**



**g**



**h**



## Supplementary figure legends

**Figure S1. Validation of automated image analysis.** (a) Histograms of mitotic exit timing based on IBB-import after anaphase onset ( $t = 0$ ) of the same dataset analysed manually (left, white bars), or automatically (right, black bars). (b) Automated annotation is highly reproducibly between movies (three independent movies shown).

**Figure S2. Validation of RNAi efficiency.** (a-c) Mitotic exit timing measured as in Figure 1, for six different siRNAs targeting CA ( $n \geq 382$  for each siRNA condition; mean $\pm$ s.d.) (a), R1A ( $n \geq 175$  for each siRNA condition) (b), or B55 $\alpha$  ( $n \geq 108$  for each siRNA condition) (c). (d-f) Quantification of mRNA knockdown 40 h post transfection by real-time PCR for the same siRNAs as in (a-c), targeting CA (d), R1A (e), or B55 $\alpha$  (f), normalized against GAPDH ( $n = 3$  for each condition; mean $\pm$ s.d.). See Supplementary Information, Table 2 for siRNA sequences. (g) Protein depletion levels of CA, R1A, and B55 $\alpha$ , detected by Western blotting in cells depleted for the indicated siRNAs 60 h post-transfection. Note that depletion of CA or R1A co-depletes other subunits of the PP2A-B55 $\alpha$  complex, consistent with previous reports<sup>39, 40</sup>. (h) Quantification of Importin  $\beta$ 1 mRNA knockdown 48 h post transfection. (i) Importin  $\beta$ 1 protein levels, detected by Western blotting 64 h after siRNA transfection. (j) Quantification of B55 $\delta$  mRNA knockdown 48 h post transfection.

**Figure S3. Phenotypes of B55 $\alpha$  single depletions.** (a) Nuclear reassembly timing in a B55 $\alpha$ -depleted cell, see also Supplementary Information, Movie S11. (b) Golgi reassembly timing in a B55 $\alpha$ -depleted cell, see also Supplementary Information, Movie S12. (c-e) Cumulative histograms of postmitotic Golgi clustering (c), chromosome decondensation (d), and spindle disassembly (e) relative to anaphase onset (0 min). Scale bars: 10  $\mu$ m.

**Figure S4. Effect of PP2A-B55 $\alpha$ -depletion on cell cycle progression.** (a) Cell cycle staging by DNA replication factor pattern of EGFP-PCNA. (b, c, d) Cumulative histograms of G1-phase (b), S-phase (c), and G2-phase (d) duration. Scale bars: 10  $\mu$ m.

**Figure S5. B55 $\alpha$  functions downstream of Cdk1-cyclin B inactivation.** (a) Movie of a cell transfected with non-silencing control siRNA, following the protocol indicated in Figure 4a. Arrowhead indicates onset of nuclear import of IBB-EGFP. (b) Time-lapse images of a cell transfected with siRNA targeting B55 $\alpha$ , see also Supplementary Information, Movie S13. (c, d) Cumulative histograms of nuclear envelope assembly (c) and Golgi clustering (d) timing based on the data shown in (a-b, and data not shown). (e) Chemical induction of mitotic exit in presence of proteasome inhibitor in nocodazole arrested mitotic cells results in rapid dephosphorylation of Cdk substrates (siControl, lanes 1-7). Cells depleted for B55 $\alpha$  show delayed dephosphorylation (siB55 $\alpha$ , lanes 8-14). Scale bars: 10  $\mu$ m.

**Figure S6. Expression levels and localization of PP2A-B55 $\alpha$ .** (a) PP2A-B55 $\alpha$  subunits are expressed at constant levels during the cell cycle. Whole cell lysates were probed by Western Blotting using the antibodies against CA, R1A, and B55 $\alpha$ . Left lane: 17 h nocodazole arrested cells (noc), right lane: unsynchronized interphase cells (log). Note that CA migrates as a doublet band (see also Supplementary Information, Figure S2g). (b) Localization of B55 $\alpha$ . Confocal live images of cells expressing EGFP-mouse-B55 $\alpha$  from endogenous promotor (see Fig. 2b). Scale bar: 10  $\mu$ m.

**Figure S7. Early mitotic progression in Importin  $\beta$ 1-depleted cells.** Timing from prometaphase until anaphase was measured for the same cells shown in Fig. 5e.

**Figure S8. Quantification of phosphorylation levels by extracted ion chromatograms.** Extracted ion chromatograms (XICs) of phosphopeptides identified (hash indicates the phosphorylated amino acid), and their unmodified counterparts, from purified PP2A complexes. Peak-area values for the phosphopeptides were used for quantification of the mitotic increase in phosphorylation abundance, whereas those of the unmodified peptides were used for normalization, as described in the legend for Fig. 5f. The panels show: 1. XIC featuring the phosphorylated peptide identified from the PP2A complex purified from interphase (log) cells. 2. XIC featuring the same phosphorylated peptide identified from the mitotic (noc) cell state. 3. XIC featuring the unmodified counterpart peptide from interphase. 4. XIC featuring the unmodified counterpart peptide from the mitotic (noc) cell state. **(a)** Quantitation of S554 phosphorylation on R1A. **(b)** S8 phosphorylation on R1A. **(c)** T304 phosphorylation on CA. **(d)** S212 phosphorylation on CA. **(e)** S167 phosphorylation on B55 $\alpha$ .

**Figure S9. Full scans of blots.** **(a)** Full scan for B55 $\alpha$  and Actin immunoblot of Figure 2b. **(b)** Full scan for phospho(Ser)Cdk substrates (upper) and Cyclin B1, Nucleolin, and Actin (lower) immunoblot of Figure 4f. **(c)** Full scan for Importin  $\beta$ 1 and R1A IP-blot (left) and Importin  $\beta$ 1 Input-blot (right) of Figure 5d. **(d)** Full scan for CA (upper left), R1A and B55 $\alpha$  (lower left), and loading control blots (right panels) of Figure S2g. **(e)** Full scan for Importin  $\beta$ 1 and Actin immunoblot of Figure S2i. **(f)** Full scan for phospho(Ser)Cdk substrates (upper) and Cyclin B1, and Nucleolin (lower) immunoblot of Figure S5e. **(g)** Full scan for CA, R1A, and B55 $\alpha$  (right) and Actin (left) immunoblot of Figure S6a. (Sliced bands are indicated with arrows). **(h)** Relevance of B55 $\alpha$ -S167 phosphorylation for PP2A complex assembly. Independent replica of the experiment shown in Fig. 5g.

## Supplementary movie legends

**Movie S1** Monoclonal fluorescent HeLa cell line expressing chromatin marker H2B-mCherry and the nuclear import substrate IBB-EGFP. The movie shows 13% of the total image size and represent a typical overnight screening movie. Time-lapse covers a period of ~21 hours.

**Movie S2** H2B-mCherry / IBB-EGFP reporter cell that has been automatically detected, tracked, and segmented over time. Movie shows original images (left); mitotic stage classification with color label as in Fig. 1c (middle), and regions of IBB measurements (right). Time-lapse covers a period of 216 minutes.

**Movie S3** H2B-mCherry / IBB-EGFP cell treated with siControl. This movie shows mitotic progression and nuclear envelope reassembly in a control cell. Time-lapse covers a period of 192 minutes.

**Movie S4** H2B-mCherry / IBB-EGFP cell treated with siPP2A-B55 $\alpha$ . This movie shows mitotic progression and delayed nuclear envelope reassembly in a cell depleted for PP2A-B55 $\alpha$ . Time-lapse covers a period of 192 minutes.

**Movie S5** H2B-mCherry / GalT-EGFP cell treated with siControl. This movie shows mitotic progression and Golgi reassembly in a control cell. Time-lapse covers a period of 132 minutes.

**Movie S6** H2B-mCherry / GalT-EGFP cell treated with siPP2A-B55 $\alpha$ . This movie shows mitotic progression and delayed Golgi reassembly in a cell depleted for PP2A-B55 $\alpha$ . Time-lapse covers a period of 161 minutes.

**Movie S7** H2B-mCherry / mEGFP- $\alpha$ -tubulin cell treated with siControl. This movie shows mitotic progression and mitotic spindle dynamics in a control cell. Time-lapse covers a period of 108 minutes.

**Movie S8** H2B-mCherry / mEGFP- $\alpha$ -tubulin cell treated with siPP2A-B55 $\alpha$ . This movie shows mitotic progression and delayed mitotic spindle disassembly in a cell depleted for PP2A-B55 $\alpha$ . Time-lapse covers a period of 108 minutes.

**Movie S9** H2B-mCherry / IBB-EGFP cell treated with siControl. This movie shows forced mitotic exit in presence of MG132 by addition of the Cdk inhibitor flavopiridol in a control cell. Time-lapse covers a period of 47 minutes.

**Movie S10** H2B-mCherry / IBB-EGFP cell treated with siPP2A-B55 $\alpha$ . This movie shows delayed mitotic exit in presence of MG132 by addition of the Cdk inhibitor flavopiridol in a cell depleted for PP2A-B55 $\alpha$ . Time-lapse covers a period of 47 minutes.

**Supplementary Information Table 1. Library of siRNA oligos**

genid	symbol	Qiagen product name	ernaAccessions	Qiagen product id	description	target	antisense	ensembl	ensembl
52	ACP1	Hs_ACP1_5	NM_004300_NM_007099_NM_177564	S026565164	acid phosphatase 1, soluble	CCTCATGTCGACATCTGTATA	UAUACAGAUUGUCACAUUUAU	CAUAGUUCGACACUUGUAU	
52	ACP1	Hs_ACP1_6	NM_004300_NM_007099_NM_177564	S027770855	acid phosphatase 1, soluble	ATGATGGAAACCAACTGTGAA	UCUACAGAUUGUCACAUUUAU	GGAUAGAACAUUACAUUUAU	
52	ACP1	Hs_ACP1_7	NM_001040949_NM_004300_NM_007099	S03068772	acid phosphatase 1, soluble	CGAAGGGATCTTGTACCCGTA	UAGUACGUUAGUACAUUUAU	GGAUAGAACAUUACAUUUAU	
52	ACP2	Hs_ACP2_5	NM_001610	S026568628	acid phosphatase 2, lysosomal	CTGGATGTCTCACAGTGTTA	UAAACACUUAUGAGACAUUUAU	GGAUAGGGCUGUAUAGGGUUA	
53	ACP2	Hs_ACP2_6	NM_001610	S026568635	acid phosphatase 2, lysosomal	CAGCGCTTGAAGTCTTCGGAAA	UUUCCGGAGAACUUCAGCGG	GCGCUAGAGUUCUUCGAAU	
53	ACP2	Hs_ACP2_7	NM_001610	S030683319	acid phosphatase 2, lysosomal	CAGAAATGAGATTCCTGGGAAT	AUUCCGAGAACUUCAGAUUUAU	GAUAGGAGAUUCUUCGAAU	
54	ACP5	Hs_ACP5_1	NM_001611	S026568642	acid phosphatase 5, tartrate resistant	GGCGGCGAGAGTCCTGAA	UAAACAGAUUGUCACAUUUAU	GGAUAGAACAUUACAUUUAU	
54	ACP5	Hs_ACP5_3	NM_001611	S026568649	acid phosphatase 5, tartrate resistant	AGCGGCGATGCTGAACTGCAA	UAGUACGUUAGUACAUUUAU	GCGCUAGAGUUCUUCGAAU	
54	ACP5	Hs_ACP5_4	NM_001611	S026568656	acid phosphatase 5, tartrate resistant	CACTGTCGACAGACATGCAA	UAGUACGUUAGUACAUUUAU	GCGCUAGAGUUCUUCGAAU	
55	ACP5	Hs_ACP5_1	NM_001099	S020021882	acid phosphatase, prostate	CTCTATTACATTATGGATAA	UAAUCCAUUAUGGUAUAUUAU	CUAUAAUCCAUUAUGGUAUAU	
55	ACP5P	Hs_ACPP_2	NM_001099	S00021889	acid phosphatase, prostate	ACAGATGGCCCTAGTGTTTA	UAAACACUUAUGAGCCAUUUAU	AGAUAGGGCUGUAUAGGGUUA	
55	ACP5P	Hs_ACPP_3	NM_001099	S00021896	acid phosphatase, prostate	CCGGAGCTTGTAGAGTGTAT	UAACACUCAUCAAGAUUUAU	GGAUAGGGUUAUAGGGUAUA	
248	ALPI	Hs_ALPI_5	NM_001631	S026565579	alkaline phosphatase, intestinal	CGAGCTTCACTCTGGCGAA	UAGUACGUUAGAAGUAGCGG	CGCUAGAGUUCUUCGAAU	
248	ALPI	Hs_ALPI_6	NM_001631	S03083157	alkaline phosphatase, intestinal	CGCGTTGAGGCCACCTCTCA	UAGUACGUUAGAAGUAGCG	GUUAGGACCUUACUCUUAU	
248	ALPI	Hs_ALPI_7	NM_001631	S030683319	alkaline phosphatase, intestinal	UAGUACGUUAGAAGUAGCG	CGAGGAGGAGAACUACAUUUAU	CGAGGAGGAGAACUACAUUUAU	
248	ALPI	Hs_ALPI_8	NM_001631	S030683319	alkaline phosphatase, intestinal	CGCGTTGAGGCCACCTCTCA	UAGUACGUUAGAAGUAGCG	GUUAGGACCUUACUCUUAU	
248	ALPL	Hs_ALPL_5	NM_002478	S026568600	alkaline phosphatase, liver/bone/kidney	CGCGTTGAGGCCACCTCTCA	UAGUACGUUAGAAGUAGCG	CGAGGAGGAGAACUACAUUUAU	
248	ALPL	Hs_ALPL_6	NM_002478	S026568607	alkaline phosphatase, liver/bone/kidney	CGAGATGGACACATCTGTTA	UAAUCCAUUAUGGUAUAUUAU	CGAGGAGGAGAACUACAUUUAU	
248	ALPL	Hs_ALPL_7	NM_002478	S026568614	alkaline phosphatase, placental-like 2	CGAGGAGCTTCTCAAGGAA	UUCGGGUUAUAGGGACGG	GCGGUUCUCUUAUAGGGAA	
251	ALPL2	Hs_ALPL2_5	NM_031313	S026569476	alkaline phosphatase, placental-like 2	TGGGGTCGAGGATGAGCTCA	UAGUACGUUAGAAGUAGCG	CGUCAGGAGGAAUAGGGUUA	
251	ALPL2	Hs_ALPL2_1	NM_031313	S026569476	alkaline phosphatase, placental-like 2	UAGUACGUUAGAAGUAGCG	CGUCAGGAGGAAUAGGGUUA	CGUCAGGAGGAAUAGGGUUA	
251	ALPL2	Hs_ALPL2_2	NM_031313	S026569476	alkaline phosphatase, placental-like 2	UAGUACGUUAGAAGUAGCG	CGUCAGGAGGAAUAGGGUUA	CGUCAGGAGGAAUAGGGUUA	
993	CCDC25A	Hs_CCDC25A_1	NM_001789_NM_001789_NM_201567	S022225454	cell division cycle 25 homolog A (S. pombe)	CGTGCAGCAATGGACATGCA	UAUACGUUAGUACAUUUAU	GCGCAAGAACUACAUUUAU	
993	CCDC25A	Hs_CCDC25A_2	NM_001789_NM_001789_NM_201567	S026569457	cell division cycle 25 homolog A (S. pombe)	CGTGCAGCAATGGACATGCA	UAUACGUUAGUACAUUUAU	GCGCAAGAACUACAUUUAU	
993	CCDC25A	Hs_CCDC25A_3	NM_001789_NM_001789_NM_201567	S026569457	cell division cycle 25 homolog A (S. pombe)	CGTGCAGCAATGGACATGCA	UAUACGUUAGUACAUUUAU	GCGCAAGAACUACAUUUAU	
994	CCDC25B	Hs_CCDC25B_10	NM_004358_NM_021872_NM_021873_NM_021873	S026569272	cell division cycle 25 homolog B (S. pombe)	CCGGAGCTTGTGAGTAGTTA	UAAUCCAUUAUGGUAUAUUAU	CGAGUAGGGUUAUAGGGUUA	
994	CCDC25B	Hs_CCDC25B_11	NM_004358_NM_021872_NM_021873_NM_021873	S026569272	cell division cycle 25 homolog B (S. pombe)	CCGGAGCTTGTGAGTAGTTA	UAAUCCAUUAUGGUAUAUUAU	CGAGUAGGGUUAUAGGGUUA	
994	CCDC25B	Hs_CCDC25B_8	NM_004358_NM_021872_NM_021873_NM_021873	S026569272	cell division cycle 25 homolog B (S. pombe)	CCGGAGCTTGTGAGTAGTTA	UAAUCCAUUAUGGUAUAUUAU	CGAGUAGGGUUAUAGGGUUA	
995	CCDC25C	Hs_CCDC25C_8	NM_001790	S026568642	cell division cycle 25 homolog C (S. pombe)	CCAGGGAGCTTAAAGCTTA	UAGUACGUUAGGCCUCCUgg	AGGGAGGCCUCCUAAUUAU	
995	CCDC25C	Hs_CCDC25C_9	NM_001790	S026568642	cell division cycle 25 homolog C (S. pombe)	CCAGGGAGCTTAAAGCTTA	UAGUACGUUAGGCCUCCUgg	AGGGAGGCCUCCUAAUUAU	
995	CCDC25C	Hs_CCDC25C_10	NM_001790	S026568642	cell division cycle 25 homolog C (S. pombe)	CCAGGGAGCTTAAAGCTTA	UAGUACGUUAGGCCUCCUgg	AGGGAGGCCUCCUAAUUAU	
1033	CDKN3	Hs_CDKN3_1	NM_005192	S026465621	cyclin-dependent kinase inhibitor 3 (CDK2-associated dual specificity phosphatase)	CTGACATGATTCATGTTA	UAGUACGUUAGGCCUCCUgg	CGAGGAGGCCUCCUAAUUAU	
1033	CDKN3	Hs_CDKN3_2	NM_005192	S026465621	cyclin-dependent kinase inhibitor 3 (CDK2-associated dual specificity phosphatase)	CTGACATGATTCATGTTA	UAGUACGUUAGGCCUCCUgg	CGAGGAGGCCUCCUAAUUAU	
1033	CDKN3	Hs_CDKN3_3	NM_005192	S026465621	cyclin-dependent kinase inhibitor 3 (CDK2-associated dual specificity phosphatase)	CTGACATGATTCATGTTA	UAGUACGUUAGGCCUCCUgg	CGAGGAGGCCUCCUAAUUAU	
1043	DUSP1	Hs_DUSP1_1	NM_004417	S03074801	dual specificity phosphatase 1	TAGCGCTGAGATTCCTGGA	UACCAAGAUUCUUCUUGACG	CGCGUACAGAACUUCUUGAC	
1043	DUSP1	Hs_DUSP1_3	NM_004417	S030748115	dual specificity phosphatase 1	CGAGGAGACAGGCTGCTGA	UAUACGUUAGGCCUCCUgg	CGAGAACUUCUUGACUUAU	
1043	DUSP1	Hs_DUSP4	NM_004417	S03074822	dual specificity phosphatase 1	CGTGGTGTGTTGCTGTTA	UAGUACGUUAGGCCUCCUgg	CGAGAACUUCUUGACUUAU	
1043	DUSP1	Hs_DUSP6	NM_004417	S03074824	dual specificity phosphatase 1	CGCGGAGCTTAAAGCTTA	UAGUACGUUAGGCCUCCUgg	CGAGAACUUCUUGACUUAU	
1043	DUSP1	Hs_DUSP7	NM_004417	S03074825	dual specificity phosphatase 1	UAGUACGUUAGGCCUCCUgg	CGAGAACUUCUUGACUUAU	CGAGAACUUCUUGACUUAU	
1043	DUSP1	Hs_DUSP9	NM_004417	S03074826	dual specificity phosphatase 1	CGCGGAGCTTAAAGCTTA	UAGUACGUUAGGCCUCCUgg	CGAGAACUUCUUGACUUAU	
1043	DUSP1	Hs_DUSP10	NM_004417	S03074827	dual specificity phosphatase 1	UAGUACGUUAGGCCUCCUgg	CGAGAACUUCUUGACUUAU	CGAGAACUUCUUGACUUAU	
1043	DUSP1	Hs_DUSP11	NM_004417	S03074828	dual specificity phosphatase 1	CGCGGAGCTTAAAGCTTA	UAGUACGUUAGGCCUCCUgg	CGAGAACUUCUUGACUUAU	
1043	DUSP1	Hs_DUSP12	NM_004417	S03074829	dual specificity phosphatase 1	UAGUACGUUAGGCCUCCUgg	CGAGAACUUCUUGACUUAU	CGAGAACUUCUUGACUUAU	
1043	DUSP1	Hs_DUSP13	NM_004417	S03074830	dual specificity phosphatase 1	CGCGGAGCTTAAAGCTTA	UAGUACGUUAGGCCUCCUgg	CGAGAACUUCUUGACUUAU	
1043	DUSP1	Hs_DUSP14	NM_004417	S03074831	dual specificity phosphatase 1	UAGUACGUUAGGCCUCCUgg	CGAGAACUUCUUGACUUAU	CGAGAACUUCUUGACUUAU	
1043	DUSP1	Hs_DUSP15	NM_004417	S03074832	dual specificity phosphatase 1	CGCGGAGCTTAAAGCTTA	UAGUACGUUAGGCCUCCUgg	CGAGAACUUCUUGACUUAU	
1043	DUSP1	Hs_DUSP16	NM_004417	S03074833	dual specificity phosphatase 1	UAGUACGUUAGGCCUCCUgg	CGAGAACUUCUUGACUUAU	CGAGAACUUCUUGACUUAU	
1043	DUSP1	Hs_DUSP17	NM_004417	S03074834	dual specificity phosphatase 1	CGCGGAGCTTAAAGCTTA	UAGUACGUUAGGCCUCCUgg	CGAGAACUUCUUGACUUAU	
1043	DUSP1	Hs_DUSP18	NM_004417	S03074835	dual specificity phosphatase 1	UAGUACGUUAGGCCUCCUgg	CGAGAACUUCUUGACUUAU	CGAGAACUUCUUGACUUAU	
1043	DUSP1	Hs_DUSP19	NM_004417	S03074836	dual specificity phosphatase 1	CGCGGAGCTTAAAGCTTA	UAGUACGUUAGGCCUCCUgg	CGAGAACUUCUUGACUUAU	
1043	DUSP1	Hs_DUSP20	NM_004417	S03074837	dual specificity phosphatase 1	UAGUACGUUAGGCCUCCUgg	CGAGAACUUCUUGACUUAU	CGAGAACUUCUUGACUUAU	
2203	FBP1	Hs_FBP1_1	NM_00507	S026564648	fructose-1,6-bisphosphatase	TTCTGAGATTCCTGTTA	UAGUACGUUAGGCCUCCUgg	CGAGAACUUCUUGACUUAU	
2203	FBP1	Hs_FBP1_6	NM_00507	S026564648	fructose-1,6-bisphosphatase	TTCTGAGATTCCTGTTA	UAGUACGUUAGGCCUCCUgg	CGAGAACUUCUUGACUUAU	
2203	FBP1	Hs_FBP1_7	NM_00507	S026564648	fructose-1,6-bisphosphatase	TTCTGAGATTCCTGTTA	UAGUACGUUAGGCCUCCUgg	CGAGAACUUCUUGACUUAU	
2203	FBP1	Hs_FBP1_8	NM_00507	S026564648	fructose-1,6-bisphosphatase	TTCTGAGATTCCTGTTA	UAGUACGUUAGGCCUCCUgg	CGAGAACUUCUUGACUUAU	
2203	FBP1	Hs_FBP1_9	NM_00507	S026564648	fructose-1,6-bisphosphatase	TTCTGAGATTCCTGTTA	UAGUACGUUAGGCCUCCUgg	CGAGAACUUCUUGACUUAU	
2203	FBP1	Hs_FBP1_10	NM_00507	S026564648	fructose-1,6-bisphosphatase	TTCTGAGATTCCTGTTA	UAGUACGUUAGGCCUCCUgg	CGAGAACUUCUUGACUUAU	
2203	FBP1	Hs_FBP1_11	NM_00507	S026564648	fructose-1,6-bisphosphatase	TTCTGAGATTCCTGTTA	UAGUACGUUAGGCCUCCUgg	CGAGAACUUCUUGACUUAU	
2203	FBP1	Hs_FBP1_12	NM_00507	S026564648	fructose-1,6-bisphosphatase	TTCTGAGATTCCTGTTA	UAGUACGUUAGGCCUCCUgg	CGAGAACUUCUUGACUUAU	
2203	FBP1	Hs_FBP1_13	NM_00507	S026564648	fructose-1,6-bisphosphatase	TTCTGAGATTCCTGTTA	UAGUACGUUAGGCCUCCUgg	CGAGAACUUCUUGACUUAU	
2203	FBP1	Hs_FBP1_14	NM_00507	S026564648	fructose-1,6-bisphosphatase	TTCTGAGATTCCTGTTA	UAGUACGUUAGGCCUCCUgg	CGAGAACUUCUUGACUUAU	
2203	FBP1	Hs_FBP1_15	NM_00507	S026564648	fructose-1,6-bisphosphatase	TTCTGAGATTCCTGTTA	UAGUACGUUAGGCCUCCUgg	CGAGAACUUCUUGACUUAU	
2203	FBP1	Hs_FBP1_16	NM_00507	S026564648	fructose-1,6-bisphosphatase	TTCTGAGATTCCTGTTA	UAGUACGUUAGGCCUCCUgg	CGAGAACUUCUUGACUUAU	
2203	FBP1	Hs_FBP1_17	NM_00507	S026564648	fructose-1,6-bisphosphatase	TTCTGAGATTCCTGTTA	UAGUACGUUAGGCCUCCUgg	CGAGAACUUCUUGACUUAU	
2203	FBP1	Hs_FBP1_18	NM_00507	S026564648	fructose-1,6-bisphosphatase	TTCTGAGATTCCTGTTA	UAGUACGUUAGGCCUCCUgg	CGAGAACUUCUUGACUUAU	
2203	FBP1	Hs_FBP1_19	NM_00507	S026564648	fructose-1,6-bisphosphatase	TTCTGAGATTCCTGTTA	UAGUACGUUAGGCCUCCUgg	CGAGAACUUCUUGACUUAU	
2203	FBP1	Hs_FBP1_20	NM_00507	S026564648	fructose-1,6-bisphosphatase	TTCTGAGATTCCTGTTA	UAGUACGUUAGGCCUCCUgg	CGAGAACUUCUUGACUUAU	
2203	FBP1	Hs_FBP1_21	NM_00507	S026564648	fructose-1,6-bisphosphatase	TTCTGAGATTCCTGTTA	UAGUACGUUAGGCCUCCUgg	CGAGAACUUCUUGACUUAU	
2203	FBP1	Hs_FBP1_22	NM_00507	S026564648	fructose-1,6-bisphosphatase	TTCTGAGATTCCTGTTA	UAGUACGUUAGGCCUCCUgg	CGAGAACUUCUUGACUUAU	
2203	FBP1	Hs_FBP1_23	NM_00507	S026564648	fructose-1,6-bisphosphatase	TTCTGAGATTCCTGTTA	UAGUACGUUAGGCCUCCUgg	CGAGAACUUCUUGACUUAU	
2203	FBP1	Hs_FBP1_24	NM_00507	S026564648	fructose-1,6-bisphosphatase	TTCTGAGATTCCTGTTA	UAGUACGUUAGGCCUCCUgg	CGAGAACUUCUUGACUUAU	
2203	FBP1	Hs_FBP1_25	NM_00507	S026564648	fructose-1,6-bisphosphatase	TTCTGAGATTCCTGTTA	UAGUACGUUAGGCCUCCUgg	CGAGAACUUCUUGACUUAU	
2203	FBP1	Hs_FBP1_26	NM_00507	S026564648	fructose-1,6-bisphosphatase	TTCTGAGATTCCTGTTA	UAGUACGUUAGGCCUCCUgg	CGAGAACUUCUUGACUUAU	
2203	FBP1	Hs_FBP1_27	NM_00507	S026564648	fructose-1,6-bisphosphatase	TTCTGAGATTCCTGTTA	UAGUACGUUAGGCCUCCUgg	CGAGAACUUCUUGACUUAU	
2203	FBP1	Hs_FBP1_28	NM_00507	S026564648	fructose-1,6-bisphosphatase	TTCTGAGATTCCTGTTA	UAGUACGUUAGGCCUCCUgg	CGAGAACUUCUUGACUUAU	
2203	FBP1	Hs_FBP1_29	NM_00507	S026564648	fructose-1,6-bisphosphatase	TTCTGAGATTCCTGTTA	UAGUACGUUAGGCCUCCUgg	CGAGAACUUCUUGACUUAU	
2203	FBP1	Hs_FBP1_30	NM_00507	S026564648	fructose-1,6-bisphosphatase	TTCTGAGATTCCTGTTA	UAGUACGUUAGGCCUCCUgg	CGAGAACUUCUUGACUUAU	
2203	FBP1	Hs_FBP1_31	NM_00507	S026564648	fructose-1,6-bisphosphatase	TTCTGAGATTCCTGTTA	UAGUACGUUAGGCCUCCUgg	CGAGAACUUCUUGACUUAU	
2203	FBP1	Hs_FBP1_32	NM_00507	S026564648	fructose-1,6-bisphosphatase	TTCTGAGATTCCTGTTA	UAGUACGUUAGGCCUCCUgg	CGAGAACUUCUUGACUUAU	
2203	FBP1	Hs_FBP1_33	NM_00507	S026564648	fructose-1,6-bisphosphatase	TTCTGAGATTCCTGTTA	UAGUACGUUAGGCCUCCUgg	CGAGAACUUCUUGACUUAU	
2203	FBP1	Hs_FBP1_34	NM_00507	S026564648	fructose-1,6-bisphosphatase	TTCTGAGATTCCTGTTA	UAGUACGUUAGGCCUCCUgg	CGAGAACUUCUUGACUUAU	
2203	FBP1	Hs_FBP1_35	NM_00507	S026564648	fructose-1,6-bisphosphatase	TTCTGAGATTCCTGTTA	UAGUACGUUAGGCCUCCUgg	CGAGAACUUCUUGACUUAU	
2203	FBP1	Hs_FBP1_36	NM_00507	S026564648	fructose-1,6-bisphosphatase	TTCTGAGATTCCTGTTA	UAGUACGUUAGGCCUCCUgg	CGAGAACUUCUUGACUUAU	
2203	FBP1	Hs_FBP1_37	NM_00507	S026564648	fructose-1,6-bisphosphatase	TTCTGAGATTCCTGTTA			







170954	KIAA1949	Hs_ KIAA1949_4	NM_133471 XM_929887 XM_934035 XM_S002824423	KIAA1949		TCCGGTCAGGCCGAGAGAAA	UUUUCUCUGGCCUCGAACGgg	CGUUCGAGCCGAGAGAAAH
201562	PTPLB	Hs_ PTPLB_5	NM_198402	protein tyrosine phosphatase-like (proline instead of catalytic arginine), member b	S002659454	CAAGGGCTACGGGGTCATGTA	UAGAUUACGGUACCGGGGgg	CGGGGACCUUGUGCAUCUAA
201562	PTPLB	Hs_ PTPLB_6	NM_198402	protein tyrosine phosphatase-like (proline instead of catalytic arginine), member b	S002659455	GGGGGGGGGGGGGGGGGGGG	GGGGGGGGGGGGGGGGGGGG	GGGGGGGGGGGGGGGGGGGG
201562	PTPLB	Hs_ PTPLB_3	NM_198402	protein tyrosine phosphatase-like (proline instead of catalytic arginine), member b	S002659453	GGGGGGGGGGGGGGGGGGGG	GGGGGGGGGGGGGGGGGGGG	GGGGGGGGGGGGGGGGGGGG
286262	Cbx7f5	Hs_ Cbx7f5_1	NM_173691	S003339695	chromosome 9 open reading frame 75	TACGCTTAACTCTCTATGGAT	AUCGUACUAGAAAAGUAGGgg	CGGUUAACUUCUUCUGCAU
286262	Cbx7f5	Hs_ Cbx7f5_2	NM_173691	S00333972	chromosome 9 open reading frame 75	CTGCTCAAAGAAAAGATGAA	UUCUACUULCUCUUCUGAGGgg	CGUCAAAAGAACAUAGAAAH
286262	Cbx7f5	Hs_ Cbx7f5_3	NM_173691	S00333979	chromosome 9 open reading frame 75	CACAGCTGGTCCCCAAAGGAA	UUCUUCUUCUUCGGGCAACCUUg	CAGUGGUGCCCAAAGGGAAH
391025	LOC391025	Hs_ LOC391025_5	NM_00131226 XM_372775	S00436859	similar to protein tyrosine phosphatase, receptor type, U isoform 2 precursor	TGCGAAATTCTTCATGGTCAT	AUGACCAUAGAAAGAAUUUCgg	GAAGAUUCUUCUACUGUCAU
391025	LOC391025	Hs_ LOC391025_6	NM_00131226 XM_372775	S00436866	similar to protein tyrosine phosphatase, receptor type, U isoform 2 precursor	CCACATGATGAGCACATGGAA	UCCAUUUGUUCUACUACAUUgg	ACAUAGAUAGGACCAUAGAA
391025	LOC391025	Hs_ LOC391025_3	NM_00131226 XM_372775	S00436873	similar to protein tyrosine phosphatase, receptor type, U isoform 2 precursor	CCCTGTGCTTATAGACGCTCA	UGAGGUUCUACAUACAUUgg	UGUCUCUCAUAAGACGCUAA
400927	LOC400927	Hs_ LOC400927_1	NM_001034843 NR_002821 XM_376010	S00546667	TPTE and PTEN homologous inositol lipid phosphatase pseudogene	TCCTTGTTTCTTCTTCTTCTT	UUCUUCUUCUUCUUCUUCUUCU	CGGGGGGGGGGGGGGGGGGG
400927	LOC400927	Hs_ LOC400927_2	NM_001034843 NR_002821 XM_376010	S00546674	TPTE and PTEN homologous inositol lipid phosphatase pseudogene	ATGGATGTTCTCTTGGATA	UACUCGAAAGAAACAUUCCgg	CGAUGUUCUUCUUCUUCUUC
400927	LOC400927	Hs_ LOC400927_3	NM_001034843 NR_002821 XM_376010	S00546674	TPTE and PTEN homologous inositol lipid phosphatase pseudogene	TCCACAGACAAACGATTAA	UUAAAUUCUUCUUCUUCUUCU	CACAGACAAACGAAUUAH

Supplementary Information Table 2. SiRNA oligos targeting PP2A-B55 $\alpha$ , B55 $\delta$ , and Importin  $\beta$ 1.

Entrez Gene ID	NCBI gene symbol	Symbol used this study	Gene Description	mRNA Accessions	siRNA Target Sequence	Qiagen Product ID	Product Name	mRNA knockdown this study
5515	PPP2CA	CA_3	protein phosphatase 2 (formerly 2A), catalytic subunit, alpha isoform	NM_002715	ACACCTCGTGAATACAATTAA	SI00041853	HS PPP2CA_3	81%
5515	PPP2CA	CA_5	protein phosphatase 2 (formerly 2A), catalytic subunit, alpha isoform	NM_002715	ATGGAACITGAGATACTCTTA	SI02225763	HS PPP2CA_5	86%
5515	PPP2CA	CA_6	protein phosphatase 2 (formerly 2A), catalytic subunit, alpha isoform	NM_002715	CAAACAACTATTGGAGCTTAA	SI02225790	HS PPP2CA_6	87%
5515	PPP2CA	CA_7	protein phosphatase 2 (formerly 2A), catalytic subunit, alpha isoform	NM_002715	TAAGACGATGTGACTGCACAA	SI04436453	HS PPP2CA_7	78%
5515	PPP2CA	CA_8	protein phosphatase 2 (formerly 2A), catalytic subunit, alpha isoform	NM_002715	ATGGTGTCTCTCGCCATCTAA	SI04436460	HS PPP2CA_8	74%
5515	PPP2CA	CA_9	protein phosphatase 2 (formerly 2A), catalytic subunit, alpha isoform	NM_002715	TACAAAGCCTCTGTCTCAA	SI04436467	HS PPP2CA_9	80%
5518	PPP2R1A	R1A_1	protein phosphatase 2 (formerly 2A), regulatory subunit A, alpha isoform	NM_014225	TCCCCATCTGGGCAAAGACAA	SI00103733	Hs PPP2R1A_1	94%
5518	PPP2R1A	R1A_5	protein phosphatase 2 (formerly 2A), regulatory subunit A, alpha isoform	NM_014225	CTGGTGTCCGATGCCAACAA	SI02225811	Hs PPP2R1A_5	91%
5518	PPP2R1A	R1A_6	protein phosphatase 2 (formerly 2A), regulatory subunit A, alpha isoform	NM_014225	ACGGCTGAACATCATCTCTAA	SI02225818	Hs PPP2R1A_6	71%
5518	PPP2R1A	R1A_7	protein phosphatase 2 (formerly 2A), regulatory subunit A, alpha isoform	NM_014225	GACCCAGGATGTGGACGTCAAA	SI04436495	Hs PPP2R1A_7	95%
5518	PPP2R1A	R1A_8	protein phosphatase 2 (formerly 2A), regulatory subunit A, alpha isoform	NM_014225	ATGCCGGTGTCTAGAGCAGAA	SI04436502	Hs PPP2R1A_8	89%
5518	PPP2R1A	R1A_9	protein phosphatase 2 (formerly 2A), regulatory subunit A, alpha isoform	NM_014225	CACCTTGACAGAGTGAAGTCAA	SI04436509	Hs PPP2R1A_9	97%
5520	PPP2R2A	R2A_1	protein phosphatase 2 (formerly 2A), regulatory subunit B, alpha isoform	NM_002717	CTCGCCGTGCTCGCACTGAA	SI00041895	Hs PPP2R2A_1	72%
5520	PPP2R2A	R2A_3	protein phosphatase 2 (formerly 2A), regulatory subunit B, alpha isoform	NM_002717	AAGCGAGACATAACCCCTAGAA	SI00041909	Hs PPP2R2A_3	76%
5520	PPP2R2A	R2A_5	protein phosphatase 2 (formerly 2A), regulatory subunit B, alpha isoform	NM_002717	CTGCAGATGATTGGGGATTA	SI02225825	Hs PPP2R2A_5	95%
5520	PPP2R2A	R2A_6	protein phosphatase 2 (formerly 2A), regulatory subunit B, alpha isoform	NM_002717	ATGGAAGGTATAGAGATCTTA	SI02225832	Hs PPP2R2A_6	94%
5520	PPP2R2A	R2A_7	protein phosphatase 2 (formerly 2A), regulatory subunit B, alpha isoform	NM_002717	CCCGGCTTTGGTGCTGATA	SI04436516	Hs PPP2R2A_7	77%
5520	PPP2R2A	R2A_8	protein phosphatase 2 (formerly 2A), regulatory subunit B, alpha isoform	NM_002717	CAGTCTCATAGCAGAGGAGAA	SI04436523	Hs PPP2R2A_8	93%
55844	PPP2R2D	B55 $\delta$	protein phosphatase 2, regulatory subunit B, delta isoform	NM_001003656 NM_018461	CAGAGACTACCTGTCGGTGA	SI00691523	Hs PPP2R2D_1	72%
55844	PPP2R2D	B55 $\delta$	protein phosphatase 2, regulatory subunit B, delta isoform	NM_001003656 NM_018461	CCGGCTCATTAAAGAACAGTGA	SI00691530	Hs PPP2R2D_2	52%
55844	PPP2R2D	B55 $\delta$	protein phosphatase 2, regulatory subunit B, delta isoform	NM_001003656 NM_018461	TTCATCCATACCGATGTAAA	SI02759148	Hs PPP2R2D_5	82%
3837	KPNB1	Importin $\beta$ 1	karyopherin (importin) beta 1	NM_002265	TCGGTTATTTGCCAAGATA	SI00035490	Hs_KPNB1_1	89%
3837	KPNB1	Importin $\beta$ 1	karyopherin (importin) beta 1	NM_002265	CAAGAACTCTTGACATCTAA	SI00035497	Hs_KPNB1_2	90%
3837	KPNB1	Importin $\beta$ 1	karyopherin (importin) beta 1	NM_002265	AAAGGGCGGAGATCGAAGACTA	SI00035504	Hs_KPNB1_3	89%

red = used for single or triple knockdown, this study.

### **Supplementary Information Table 3. Plasmids generated for this study**

For efficient generation of cell lines stably expressing fluorescently tagged marker proteins, the genes were subcloned into pIRES-puro2 and pIRES-neo3 vectors (Clontech) that allow expression of resistance genes and tagged proteins from a single transcript.

**Table 3. Generated plasmids**

Plasmid name	Tag	Source plasmids	Vector backbone	Backbone cloning sites
pIBB-mEGFP-IRES-puro2b	mEGFP <sup>1</sup>	pIBB-mEGFP <sup>2</sup>	pIRES-puro2b	EcoRI/NotI
pGalT-GFP-IRES-puro2b	GFP	pGalT-GFP (MluI blunted/EcoRI) <sup>3</sup>	pIRES-puro2b	(NotI blunted/EcoRI)
pEGFP-PCNA-IRES-puro2b	mEGFP <sup>1</sup>	pNLS-EGFP-PCNA <sup>4</sup>	pIRES-puro2b	(NdeI, XbaI)

mEGFP indicates monomeric EGFP.

### **Supplementary Information Table 4. Monoclonal fluorescent reporter cell lines**

Stable cell lines were generated as described in <sup>5</sup>.

**Table 4. HeLa Kyoto monoclonal cell lines**

Background	Cell line name	Plasmid 1	Plasmid 2
HeLa ‘Kyoto’	H2B-mCherry	pH2B-mCherry-IRES-neo3	-
HeLa ‘Kyoto’	H2B-mCherry and IBB-mEGFP	pH2B-mCherry-IRES-neo3	pIBB-mEGFP-IRES-puro2b
HeLa ‘Kyoto’	H2B-mCherry and GalT-GFP	pH2B-mCherry-IRES-neo3	pGalT-GFP-IRES-puro2b
HeLa ‘Kyoto’	H2B-mCherry and PCNA-mEGFP	pH2B-mCherry-IRES-neo3	pPCNA-mEGFP-IRES-puro2b
HeLa ‘Kyoto’	H2B-mCherry and mEGFP-α-tubulin <sup>6</sup>	pH2B-mCherry-IRES-neo3	pmEGFP-α-tubulin-IRES-puro2b

### **Supplementary references**

1. Snapp, E.L. *et al.* Formation of stacked ER cisternae by low affinity protein interactions. *J Cell Biol* **163**, 257-269 (2003).
2. Dultz, E. *et al.* Systematic kinetic analysis of mitotic dis- and reassembly of the nuclear pore in living cells. *J Cell Biol* **180**, 857-865 (2008).
3. Schaub, B.E., Berger, B., Berger, E.G. & Rohrer, J. Transition of galactosyltransferase 1 from trans-Golgi cisterna to the trans-Golgi network is signal mediated. *Mol Biol Cell* **17**, 5153-5162 (2006).
4. Leonhardt, H. *et al.* Dynamics of DNA replication factories in living cells. *J Cell Biol* **149**, 271-280. (2000).
5. Schmitz, M. & Gerlich, D. Automated live microscopy to study mitotic gene function. *Methods in Molecular Biology*, In press (2007).
6. Steigemann, P. *et al.* Aurora B-mediated abscission checkpoint protects against tetraploidization. *Cell* **136**, 473-484 (2009).